

Effect of bi-functionalization of algal/polyethyleneimine composite beads on the enhancement of tungstate sorption: Application to metal recovery from ore leachate

Mohammed Hamza, Khalid A.M. Salih, Kanggen Zhou, Yuezhou Wei, Hanaa Abu Khoziem, Saad Alotaibi, Guibal Eric

▶ **To cite this version:**

Mohammed Hamza, Khalid A.M. Salih, Kanggen Zhou, Yuezhou Wei, Hanaa Abu Khoziem, et al.. Effect of bi-functionalization of algal/polyethyleneimine composite beads on the enhancement of tungstate sorption: Application to metal recovery from ore leachate. Separation and Purification Technology, 2022, 290, pp.120893. 10.1016/j.seppur.2022.120893 . hal-03621715

HAL Id: hal-03621715

https://imt-mines-ales.hal.science/hal-03621715

Submitted on 28 Mar 2022

HAL is a multi-disciplinary open access archive for the deposit and dissemination of scientific research documents, whether they are published or not. The documents may come from teaching and research institutions in France or abroad, or from public or private research centers.

L'archive ouverte pluridisciplinaire **HAL**, est destinée au dépôt et à la diffusion de documents scientifiques de niveau recherche, publiés ou non, émanant des établissements d'enseignement et de recherche français ou étrangers, des laboratoires publics ou privés.

Effect of bi-functionalization of algal/polyethyleneimine composite beads on the enhancement of tungstate sorption: Application to metal recovery from ore leachate

Mohammed F. Hamza [a,b], Khalid A.M. Salih [c], Kanggen Zhou [c], Yuezhou Wei [a,d,*], Hanaa A. Abu Khoziem [b], Saad H. Alotaibi [e], Eric Guibal [f,*]

[a] School of Nuclear Science and Technology, University of South China, Heng Yang 421001, China
[b] Nuclear Materials Authority, POB 530, El-Maadi, Cairo, Egypt
[c] School of Metallurgy and Environment, Central South University, Changsha 410083, China
[d] School of Nuclear Science and Engineering, Shanghai Jiao Tong University, Shanghai, China
[e] Department of Chemistry, Turabah University College, Taif University, P.O. Box 11099, Taif 21944, Saudi Arabia
[f] Polymers Composites and Hybrids (PCH), IMT Mines Ales, Alès, France

A B S T R A C T

Algal/polyethyleneimine composite beads (A_LPEI) have been successfully functionalized by grafting phospho-nate (A_LPEI-P), quaternary ammonium groups (A_LPEI-Q), and by dual moieties (A_LPEI-PQ). The materials are characterized by a wide diversity of analytical methods: SEM and SEM-EDX, TGA, BET, FTIR and XPS, elemental analysis and titration (detailed discussion in Supplementary Information). FTIR and XPS analyses show contri-butions of quaternary ammonium, hydroxyl, and phosphonate groups in tungstate binding (which may involve polynuclear species, depending on the pH). The synergistic effects of phosphonate and quaternary ammonium moieties contribute to strongly increase W(VI) sorption capacity up to 1.8 mmol W g^{-1} (i.e., 4-times compared with pristine beads), at pH 5. The strong increase of sorption properties with temperature (2.45 mmol W g^{-1} at T: 50 °C) demonstrates the endothermic nature of metal binding, which is spontaneous (and characterized by positive entropy change). The Langmuir Dual Site equation successfully fits sorption isotherm for functionalized sorbents (bearing phosphonate and phosphonate/quaternary ammonium groups in addition to proper reactive groups of pristine beads) contrary to the isotherms for raw beads (fitted by Langmuir equation). The pseudo-first order rate equation fits kinetics (equilibrium reached within ≈60 min). The bi-functional sorbent shows marked preference for W(VI) against base and alkali-earth metals (especially at pH close to 3.5). These properties are confirmed in the treatment of raffinate solutions (after ore leaching and solvent extraction): despite the complexity of the effluent, A_LPEI-PQ reveals highly efficient for W(VI) recovery and separation. The sorbent can be used as a polishing treatment for enhancing the recovery of strategic metals. Sorbed tungstate is readily desorbed from the sorbent using 0.2 M NH_4Cl solution. The sorbent is efficiently recycled for at least 5 cycles (complete desorption, loss in sorption performance less than 4% at the fifth cycle).

Keywords:
Bi-functionalization of algal/PEI beads for W (VI) enhanced sorption
Sorption isotherms and uptake kinetics
Selective recovery of W(VI) and Nb(V) from complex solutions
Remarkable stability in desorption efficiency and sorbent recycling
Efficient application to ore leachate

1. Introduction

Historically, tungsten was used for manufacturing incandescent lamps, making profit of the high melting point of the metal. The poor energy efficiency of these lamps progressively caused their replacement with more efficient systems (like led, fluorescent, halogen lamps, etc.). Nowadays, tungsten is essentially used for designing alloys for high-temperature applications. Tungsten carbide is also frequently employed for manufacturing hard cutting and drilling tools for metallurgy, mining, and petroleum industries. The main mineral resources for tungsten are scheelite ($CaWO_4$, associated with Mo, Nb and Ta impurities) and wolframite (iron, manganese, magnesium tungstate). The main producers and stock holders are China, Russia, Bolivia and USA, which concentrate more than 80% of resources. The relative supply risk is evaluated to 9.5 (the highest risk being ranked 10) [1]. The rate of recycling is estimated between 10% and 30%. This may explain that

* Corresponding authors.
E-mail addresses: yzwei@usc.edu.cn (Y. Wei), eric.guibal@mines-ales.fr (E. Guibal).

strong incentive have been enacted for promoting the recycling of strategic resources and for decreasing the environmental impact of metal uses [2–6].

Tungsten extraction from ores and wastes may involve leaching processes [7–10] (eventually associated with pyro-metallurgical techniques [11]). Several techniques have been reported for concentrating and extracting tungsten from leachates, including liquid membranes [12], and solvent extraction systems [13–16]. Playing with the characteristics of ionic liquids and precipitation, Papaiconomou and Viboud [17] showed the possibility to separate tungstate from polytungstate species. The solvent extraction techniques are highly efficient and competitive for the treatment of effluent containing high concentrations of target metals. However, sorption processes are generally more appropriate for diluted effluent. This is typically the case for the residues of solvent extraction operations, where sorption allows recovering additional amounts of metals and decreasing environmental impact in the global process. A wide range of materials may be used for recovering valuable or toxic metal ions (including tungsten) from dilute solutions including mineral-based sorbents [18–25], activated carbon [26], carbon nanotubes [27], functionalized synthetic fibers [28], and metal-organic framework [29]. Chelating resins [30–33] and ion-exchangers [31,34–37] have also retained a great attention for the last decades. The possibilities of biosorbents have also been explored for metal binding [38,39] and for tungsten recovery [40–43]; playing with the presence of reactive groups at the surface of biosourced materials (functional groups analogues to those present on synthetic resins). The biosorbents can be also functionalized to improve metal binding through grafting of complementary reactive groups, such as aminophosphonate [44].

Recently, a "collection" of new sorbents has been developed based on the functionalization of a composite material constituted of brown algal biomass and polyethyleneimine (PEI) (i.e., A_LPEI). The interactions of carboxylate groups on the algal biomass (alginate fraction) and protonated amine groups (on PEI), eventually completed by the glutaraldehyde crosslinking of PEI, leads to the formation of stable interpenetrated networks, conditioned as hydrogel beads [45]. Both alginate and PEI have shown attractive intrinsic potentialities for metal binding and/or complexation [46,47]. In the composite, the coexistence of hydroxyl, carboxyl, and amine groups makes the material very reactive for metal ions but also readily available for functionalization. For example, the sorbent was amidoximated [48], phosphorylated [49], quaternized [50], and sulfonated [51] for the recovery of a series of valuable metal ions. These functionalized sorbents are enriched with specific reactive groups though some sites present on the raw material remain available for metal sorption and/or for complementary functionalization.

Several studies have shown the interest of bi-functionality for improving sorption properties, expanding the pH range for efficient metal sorption, or for enhancing separation properties [52–57]. For example, Alexandratos and Natesan [58] reported the usefulness of associating a recognition ligand to an access ligand for promoting rare earth sorption. Alexandratos [59] also identified the beneficial impact of intraligand cooperation on sorption performance. Modulating the acidity/basicity of the sorbent may increase the sorption performance [60]; for example, the vicinity of hydroxyl groups with phosphoryl oxygen is favorable for uranyl sorption. Alexandratos and Zhu [60] claim the possibility to tune metal ion affinity playing with polarizability for designing efficient and selective sorbents. Wei et al. [61] demonstrated that the synergistic effects of protonation and amidoximation of the resin improve both the kinetics and selectivity of the sorbent for U(VI) sorption. Piechowicz et al. [62] also reported the enhanced reactivity of bi-functional resin for U(VI): carboxyl group and amidoxime ligands cooperate for metal binding.

These beneficial effects of bi-functionalization are investigated in this work comparing the sorption properties of A_LPEI (as the reference and raw support), A_LPEI-P (phosphorylated derivative of raw sorbent), A_LPEI-Q (quaternized beads), and A_LPEI-PQ (bi-functional sorbent based on the quaternization of phosphorylated derivative) for W(VI) recovery. The sorption mechanisms are investigated using FTIR and XPS spectrometry; in addition, textural, TGA, and titration analyses are used for characterizing the materials. The sorption properties are compared through the study of the effect of pH, uptake kinetics and sorption isotherms to demonstrate the enhancing effects of the bi-functionalization. The effect of competitor ions is carried out for evaluating metal selectivity (in function of pH). Tungstate desorption from metal-loaded sorbent is investigated, including kinetic profiles and sorbent recycling. The final part of the work focuses on the application of the sorbent for tungstate recovery from solvent extraction residues (applied to alkaline leachate of Egyptian W-bearing ore).

2. Materials and methods

2.1. Materials

Laminaria digitata (brown algae) was purchased from Setalg (Pleubian, France). PEI (branched; 50%, w/w in water), sodium tungstate dihydrate (≥99%) and glutaraldehyde were supplied by Sigma-Aldrich (Taufkirchen, Germany). Calcium chloride ($CaCl_2$), zinc oxide (used in selectivity tests) and sodium carbonate (Na_2CO_3) were purchased from Chem-Lab NV (Zedelgem, Belgium). Glycidyltrimethylammonium chloride (≥95%) and poly(ethylene glycol diglycidyl ether) (PEGDGE) were supplied by Shanghai Makclin Biochemical Co., Ltd. (Shanghai, China). $Nd_2(SO_4)_3$ (used in selectivity tests) was supplied by National Engineering Research Centre of Rare Earth Metallurgy and Functional Materials Co., Ltd (Baotou, China). Tributyl phosphate (TBP, $C_{12}H_{27}O_4P$), was provided by Aladdin Industrial Corporation, (Shanghai, China). Aluminum sulfate octadecahydrate, sodium hydroxide, and absolute ethanol were supplied by Guangdong Guanghua Sci-Tech Co. (Guangzhou, China). Phosphoric acid was provided by Xilong Scientific Co., (Guangdong, China). All other reagents are Prolabo products, which were used as received.

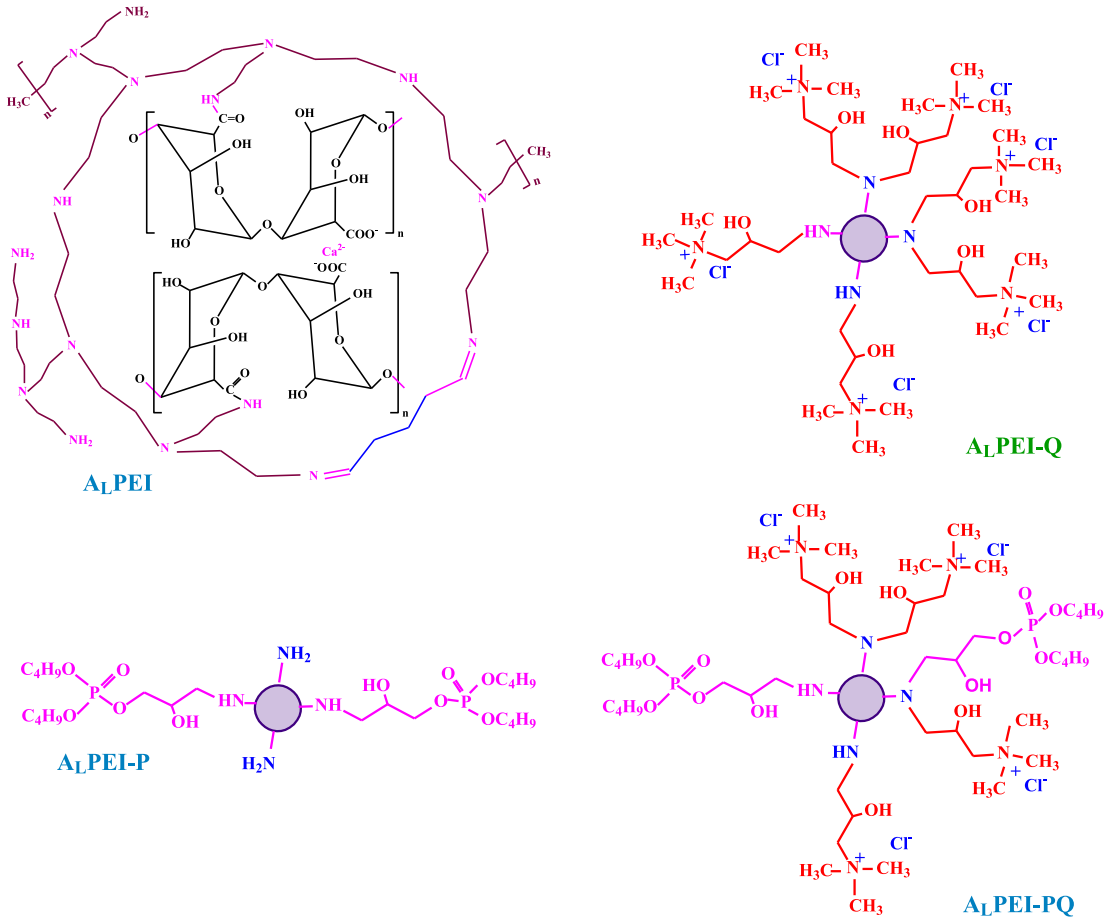
2.2. Synthesis of sorbents

The synthesis procedures are detailed in Supplementary Information (Section S1, Scheme S1). The synthesis of A_LPEI beads (pristine support) was already described [51]: alginate was (partially) thermally extracted from algal biomass with sodium carbonate before reacting with PEI (amine groups from PEI with carboxylate groups of alginate) before dropping the mixture through a nozzle into $CaCl_2$ solution (for the ionotropic gelation of carboxylate groups of the biopolymer).

The quaternization of A_LPEI beads (A_LPEI-Q) was performed by reaction of pristine beads with glycidyltrimethyl ammonium chloride [63]. The synthesis of A_LPEI-P consisted of the synthesis of dibutyl-(3-chloro-2-hydroxy)-propyl phosphate, followed by the grafting of this TBP-derivative onto A_LPEI. The bi-functionalization of A_LPEI (to obtain A_LPEI-PQ) was obtained by quaternization of A_LPEI-P using the same procedure described for direct quaternization of pristine beads. Scheme 1 reports the suggested structures of synthesized sorbents.

2.3. Characterization of sorbents

The elemental analysis of the sorbents (i.e., A_LPEI, A_LPEI-P and A_LPEI-PQ beads) was performed for C, N, O, P contents using an element analyzer-Vario EL cube (Elementar Analysensysteme GmbH, Langenselbold, Germany). An ESCALAB-250XI+- instrument (Thermo Fischer Scientific, Inc., Waltham, MA, USA) was used for XPS analyses. FTIR spectrometry was performed on dried samples through IRTracer 100 (Shimadzu, Tokyo, Japan) after being lixed with KBR and conditioned as KBr discs. A Netzsch STA-449 F3 Jupiter (NETZSCH-Gerätebau GmbH, Selb, Germany) was used for thermogravimetric analyses (TGA) under N_2 atmosphere, with temperature ramp: 10 °C/min. The pH-drift



Scheme 1. Suggested structures for A_LPEI, A_LPEI-Q, A_LPEI-P, and A_LPEI-PQ.

method was used for determining the pH_{PZC} values. One hundred mg of sorbent were mixed with 0.1 M NaCl solutions (50 mL), with pH_0 initially adjusted between 1 and 11. The final pH (pH_{eq}) was measured using a Mettler Toledo-pH meter (Mettler, Colombus, OH, USA). The pH_{PZC} is determined as the value corresponding to $pH_0 = pH_{eq}$. Morphological characterization (through SEM) and semi-quantitative energy dispersive X-ray analysis (EDX) were performed using Phenom ProX scanning electron microscope (Thermo Fisher Scientific, Netherlands) equipped with EDX facilities. Textural analysis of A_LPEI and A_LPEI-PQ beads was performed on Micromeritics TriStar II (Norcross, GA, USA), after pre-treatment (degassing at 120 °C for 12 h, before analysis). The BJH method was used for the evaluation of both specific surface area and pore size distribution.

2.4. Sorption tests

2.4.1. Experimental procedures

Sorption experiments were performed in batch system using an agitated tank reactor (agitation speed, *v*, 210 rpm). A fixed volume of solution (*V*, L) at given initial metal concentration (C_0, mmol W L^{-1}) and fixed initial pH value (pH_0) was mixed with a fixed amount of sorbent (*m*, g; sorbent dose, *SD* = m/V, g L^{-1}) for given contact times (*t*, min). After fixed contact time, a sample of solution was collected and filtrated on a 1.2 μm pore size membrane and the filtrate was analyzed for residual metal concentration ($C(t)$ or C_{eq}, mmol W L^{-1}) using ICP-AES (ICPS-7510-Shimadzu, Japan), after filtration using 1.2 μm pore size filter membrane; the equilibrium pH was systematically monitored (pH_{eq}, no pH-control during sorption process). The sorption capacity (q_{eq}, mmol W g^{-1}) was deduced by the mass balance equation: $q_{eq} = (C_0 - C_{eq}) \times V/m$. Similar procedures were used for investigating metal sorption from multi-component equimolar solutions (and tests on real complex solutions). The selectivity coefficient ($SC_{Me1/Me2}$) was calculated as the ratio D_{Me1}/D_{Me2} (where D is the distribution ratio, $D = q_{eq}/C_{eq}$):

$$SC_{Me1/Me2} = \frac{D_{Me1}}{D_{Me2}} = \frac{q_{eq,1} \times C_{eq,2}}{C_{eq,1} \times q_{eq,2}} \quad (1)$$

Desorption studies were also performed in batch systems. Metal-loaded sorbents were collected from uptake kinetics. After careful rinsing with demineralized water, the sorbents were mixed with the eluent solution (0.2 M HCl solution) for a given contact time, before analyzing the concentration of released metal ions. Before recycling the sorbent, the material was rinsed with demineralized water and the sorption properties were compared using the same experimental conditions for five successive cycles of sorption and desorption.

Note: experimental conditions are systematically reported in the caption of relevant figures. Experiments were duplicated. The experimental profiles are reported in the core of the manuscript or in the Supplementary Information to show the reproducibility of sorption performances.

2.4.2. Modeling

Uptake kinetic and sorption isotherms were fitted using conventional equations:

(a) the pseudo-first order and pseudo-second order rate equations (PFORE and PSORE), and the resistance to intraparticle diffusion (RIDE) [64,65],
(b) the Langmuir, Freundlich, Sips and Temkin equations [66,67].

The facilities of non-linear regression analysis of Mathematica® software were used for determining the parameters of the different models. The relevant equations are reported in Supplementary Information. The quality of fits was evaluated (and compared) using the determination coefficient (i.e., R^2) and the Akaike information criterion (AIC) [68].

2.5. Application to ore treatment

2.5.1. Ore treatment

Annex A (in SI) describes the location of ore deposit (Gabal Qash Amir area, Southwestern Desert, Egypt, Figure A1), the geological context (invaded quartz vein / muscovite granite), and the geochemical characteristics of the investigated ore. The grinded and sieved ore (size < 1 mm) was pre-treated through successive concentration steps using shaking and magnetic tables; the hubnerite concentrate ($MnWO_4$, more than 87% w/w, see Composition in Table A1, Figures A2 and A3) was used for hydrothermal leaching steps: (a) first, HCl acid leaching for Fe and Mn extraction (more than 99% and 94%, respectively, see composition of residue in Table A2), and (b) NaOH alkaline leaching (99 % W leaching). The detailed characterization of concentrates (and their treated residues) are reported in Annex A.

The composition of the alkaline leachate is reported in Table A3 (XRD diffractogram in Figure A4). The alkaline leachate was treated by solvent extraction using Alamine 336 (trioctylamine), in the presence of octanol as the modifier. The extraction efficiency (under selected experimental conditions) reached 94%. The stripping efficiency was close to 98%, using ammonia solution. This concentrate was valorized by evaporation at 50 °C and crystallization of pure ammonium paratungstate (99.97%, converted to WO_3 at 750 °C); the recovery yield attained 90% during the crystallization step.

Residual tungsten-loaded Alamine 336 phase was scrubbed with demineralized water for removing Na and Si impurities. The raffinate and scrubbed solutions were mixed for investigating: (a) the sorption properties of A_LPEI-PQ on complex solutions, (b) complementary W(VI) valorization, and (c) decontamination of residues. Table A4 reports the composition of the effluent tested for W(VI) sorption.

2.5.2. Tungstate recovery from residues of liquid/liquid extraction of alkaline leachates

The sorption of W(VI) (main target) was investigated using the batch process. Sorbent dose was set to 1 g L^{-1}; the contact time fixed to 10 h. Experiments were performed at room temperature (T: 22 ± 1 °C), under standard agitation (i.e., 210 rpm). The pH_0 was adjusted to different pH values (between 3 and 7). The residual concentrations were analyzed for calculating the sorption capacities, the distribution ratios (D,), and the selectivity coefficients ($SC_{W/Metal}$).

3. Results and discussion

3.1. Summary of characterization of sorbents

The detailed characterization of the sorbents is presented and discussed in the Supplementary Information (Section 2). Optical microscopy allowed evaluating the average size of sorbent beads: 2.25 ± 0.02 mm, 2.12 ± 0.10 mm, and 2.06 ± 0.16 mm for A_LPEI, A_LPEI-P, and A_LPEI-PQ, respectively. Figure S1 shows the roughly spherical shape of the beads and the irregular surface (resulting from shrinking during the sorption steps). Figure S2 shows N_2 sorption and desorption curves for the BET determination of textural properties: the specific surface area (S_{BET}) increases with the functionalization of the beads: 13.1 $m^2\ g^{-1}$ (for A_LPEI), 24.7 $m^2\ g^{-1}$ (for A_LPEI-P), and up to 42.0 $m^2\ g^{-1}$ (for A_LPEI-PQ).

FTIR and XPS spectral methods allow characterizing both the functional groups progressively grafted onto pristine beads and their interactions with tungstate species. First, the phosphorylation of pristine beads (A_LPEI-P) is demonstrated by the appearance of characteristic phosphonate bonds such as P = O asymmetric stretching and P-O-C stretching bands (at ≈ 1320 cm^{-1} and 876 cm^{-1}, respectively), and the strong band at 1425 cm^{-1} (C-H asymmetric stretching of P-O-C_4H_9) (Figure S3, Table S1). The quaternization of the sorbent (A_LPEI-PQ) induces: (a) the decrease of the relative intensity of the phosphonate bands, (b) the appearance of bands at 1463 and 1409 cm^{-1} (C-H stretching from quaternary ammonium salt moieties), and (c) the appearance of a new band at 974 cm^{-1}. Figure S4 and Tables S2-S4 show the effect of metal sorption and sorbent recycling on FTIR spectra and the assignment of relevant bands (see the main conclusions in section 3.2.4. and extensive discussion in Supplementary Information). The bi-functionalization of pristine beads is also confirmed by XPS analysis (Fig. 1, Figure S5 and Table S5). The phosphorylation is characterized by the appearance of P 2p signal in the survey XPS spectra, and in high resolution spectra by the changes in the binding energies and atomic fractions of O 1s (phosphonate grafting), N 1s signals (modification of the chemical environment of amine groups). The effective quaternization is also confirmed by the reinforcement of the signal associated with quaternary ammonium salt: a strong band appears at BE: ≈402 eV. Metal binding is characterized by the appearance of W 4f, W 4d and W 4p signals in Fig. 1 (XPS survey curves), while Figures S6-S8 (and Table S5) compare the high-resolution XPS spectra of selected signals for A_LPEI and A_LPEI-PQ sorbents before and after tungstate sorption. Elemental analysis (Table S6) shows the phosphorylation of A_LPEI (1.39 mmol P g^{-1} in A_LPEI-P), the quaternization of A_LPEI (increase of N content from 3.13 to 5.98 mmol N g^{-1} in A_LPEI-P). The bi-functionalization (in A_LPEI-PQ) increases N content from 3.13 to 5.67 mmol N g^{-1} (comparable to A_LPEI-Q), and P content up to 1.35 mmol P g^{-1} (comparable to A_LPEI-P). Figure S9 shows the SEM photographs and semi-quantitative EDX analysis of the surface of sorbent beads; A_LPEI-P seems to be more porous (largest surface holes). The sorption of W(VI) onto A_LPEI-PQ is confirmed by the semi-quantitative EDX analysis (Figure S10), while after metal desorption tungsten totally disappears from sorbent surface (the elemental composition at the surface is restored). The thermogravimetric analysis of the materials is reported in Figure S11: the phosphorylation increases the stability of the material (total weight loss does not exceed 64%, contrary to 86.7% for A_LPEI). Grafting phosphorous element is a well-known method for increasing the thermal stability of fire-retardant materials. However, the bi-functionalization decreases again when the intermediary phosphonated derivative is quaternized (total weight loss reaches 72.8%). The titration of the sorbents (to determine the pH_{PZC} values) shows the scaling in the acidification of the sorbents (Figure S12). Hence, the pH_{PZC} values range according to: A_LPEI (7.36) > A_LPEI-P (6.74) > A_LPEI-PQ (5.78) > A_LPEI-Q (5.24). This means that all the sorbents are protonated below pH 5.2; this is favorable to the electrostatic attraction of metal anions. The protonation increases with quaternization while phosphonate groups bring additional chelating properties.

3.2. Sorption properties

3.2.1. Effect of pH

The pH is a critical parameter for designing a sorption process because this parameter may control both the surface properties of the sorbent (protonation/deprotonation of reactive groups, with attraction or repulsion effects) and the speciation of metal ions (formation of precipitates, hydrolyzed species and complexes, and/or formation of polynuclear species). Fig. 2 shows the evolution of W(VI) sorption capacity *vs.* equilibrium pH for A_LPEI, A_LPEI-P, A_LPEI-Q and A_LPEI-PQ sorbents (under comparable experimental conditions). Duplicate experiments confirm the good experimental reproducibility of sorption tests. This figure clearly demonstrates the benefits of successive functionalization steps. The sorption of tungstate with A_LPEI is hardly affected by pH_{eq} (in the range 3–6.5): the sorption capacity linearly increases from 0.08 to 0.15 mmol W g^{-1}. The reactive groups present on the sorbent, which is positively charged on the full pH range (with

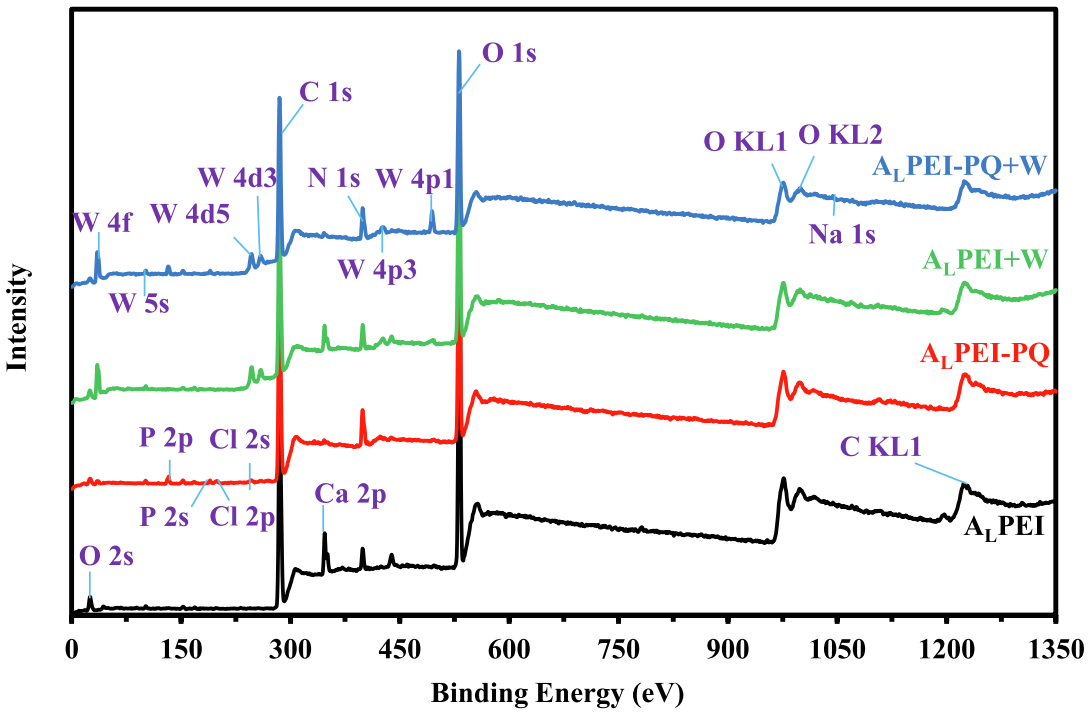


Fig. 1. XPS core level spectra of A_LPEI and A_LPEI-PQ sorbents before and after W(VI) sorption.

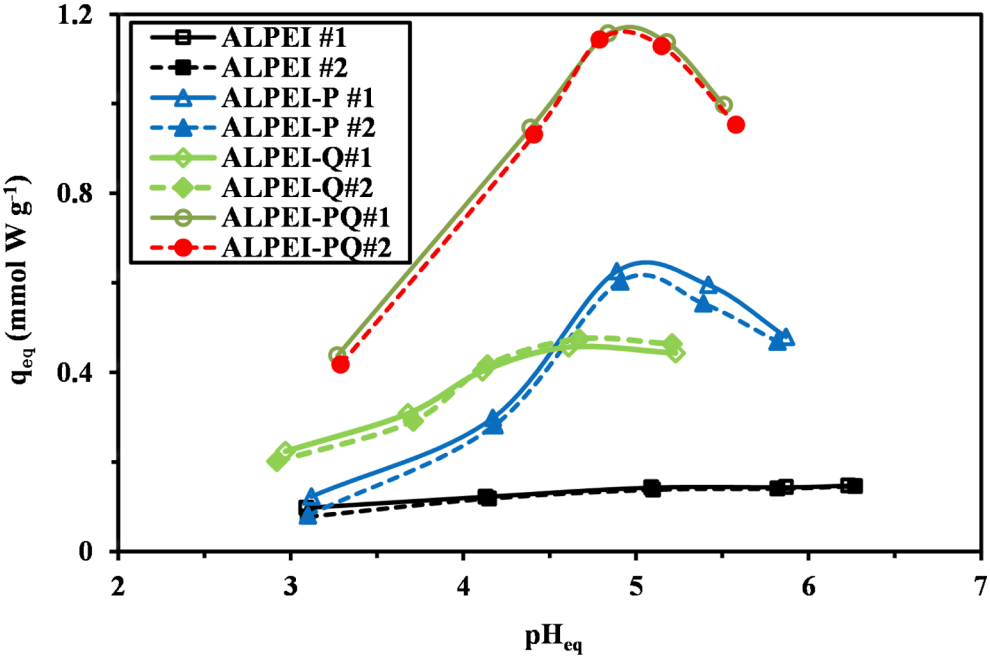


Fig. 2. Effect of pH on W(VI) sorption using A_LPEI, A_LPEI-P, A_LPEI-Q, and A_LPEI-PQ (C_0: 0.275 mmol W L^{-1}; Sorbent dose, SD: 0.4 g L^{-1}; v: 210 rpm; time: 48 h; T: 22 ± 1 °C, duplicated series: #1 and #2).

pH_{PZC}: 7.36), may explain the possibility to bind tungstate anions. However, the presence of carboxylic acid groups (from alginate) with pK_a values of 3.68–3.35 and amine groups (from PEI) with pK_a values close to 4.5, 6.7 and 11.6 mean that tungstate anions will be bound to free amine groups. The relatively weak sorption may be explained by the limited availability of these amine groups that are engaged in interactions with carboxylate groups. The grafting of phosphonate moieties strongly increases W(VI) sorption ability; under selected experimental conditions, at the optimum pH_{eq} (i.e., around 5) the sorption capacity reaches 0.6 mmol W g^{-1}. The pH_{PZC} value of A_LPEI-P is close to 6.74, meaning that in the whole range of pH investigated for W (VI) uptake the global positive charge of the sorbent remains favorable to the electrostatic attraction of tungstate anions. In acidic solutions, the competition of nitrate anions (HNO_3 has been used for pH control) may explain the low sorption efficiency of the phosphorylated sorbent. With the increase of the pH, the competition effect decreases and the binding of W(VI) is enhanced. However, at pH_{eq} above 5, the sorption capacity progressively decreases; this means that sorption is controlled by another mechanism or criterion. The speciation diagram of W(VI) (under the experimental conditions selected for pH study, and calculated

using the stability constants reported by Baes and Mesmer, [69]) shows that up to pH 4.5 the predominant species is $W_{12}O_{39}^{6-}$ (a polynuclear species) (Figure S13). However, above pH 4.5, the fraction of WO_4^{2-} (free mononuclear species) progressively increases (and predominates above pH 5). Sorption is favored by the presence of polynuclear anionic species. Binding a single polynuclear mole allows binding 12 W(VI) moles. Similar affinity for polynuclear species has already been reported in the case of molybdate and vanadate species using chitosan-based sorbents [70]. The sorption may engage the formation of poly-tungstate/phosphonate complexes [71]. Apparently, this mechanism is not active in acidic solution: the sorption capacity at pH 3 is identical to the sorption level reached with raw material (A_LPEI). With the direct quaternization of A_LPEI (A_LPEI-Q), the sorption in acidic solutions is higher than with the raw material (i.e., 0.2 mmol W g^{-1}) and progressively increases to 0.47 mmol W g^{-1} at $pH_{eq} \approx 4.7$ before slightly decreasing at pH_{eq} 5.2. Quaternary ammonium groups essentially contribute in the acid pH range to W(VI) binding. In the case of A_LPEI-PQ, the quaternization offers complementary reactive groups to phosphonate moieties; quaternary ammonium moieties, which have strong affinity for W(VI) anions that are probably associated with an ion-exchange mechanism. The bi-functional sorbent cumulates ion-exchange from amine and quaternary ammonium groups and chelating abilities of phosphonate moieties. At the optimum pH (identical to A_LPEI-P; i.e., $pH_{eq} \approx 5$), the sorption capacity increases up to 1.14 mmol W g^{-1}. The predominant species are bearing 6 anionic charges per polynuclear species, three times more than the predominant species at $pH_{eq} > 5$ (i.e., for WO_4^{2-}). This may be correlated with the stronger decrease in the sorption capacity at near neutral pH (compared with A_LPEI-P sorbent). This is confirmed by the analysis of the $\log_{10}$ plots of the distribution ratios against pH_{eq} (Figure S14a). The combination of different mechanisms (especially for the bi-functional sorbent) makes complex the interpretation of the slopes (frequently used for analyzing the stoichiometric ratio between metal ions and reactive groups, and/or the proton exchanges). However, these plots allow highlighting the sensitivity of the different systems against pH. The dual functionalization clearly enhances W(VI) sorption by synergistic (a) complexation of tungstate with phosphate groups, and (b) ion exchange of phosphonate anions with quaternary ammonium groups.

Figure S14b shows the pH variations associated with the different sorbents during W(VI) sorption. A_LPEI sorbent shows the weakest effect in terms of pH variation (probably due to acid-base properties and pH_{PZC} values, and to the weaker sorption affinity for W(VI)): the equilibrium pH varies by less than 0.2 pH unit (except at pH 7). The other sorbents show largest pH variations (increasing with the functionalization of the sorbent and consistently with pH_{PZC} values). Below pH_0 4.5, the pH tends to increase, while above, a reciprocal trend is observed. At pH 6, the pH decrease reaches 0.6 pH unit for A_LPEI-P and up to 0.85 pH unit for A_LPEI-PQ: metal sorption is followed by proton release and/or OH binding (possibly through the binding of hydrolyzed species around pH 5 (such as $W_6O_{20}(OH)^{5-}$). It is noteworthy that pH variation is the same (superposition of curves) for A_LPEI-Q and A_LPEI-PQ; the predominant impact of quaternary ammonium groups is clearly demonstrated against phosphonate moieties regarding proton exchange.

3.2.2. *Uptake kinetics*

The kinetics of sorption may be controlled by a series of diffusion mechanisms, including resistance to bulk diffusion and film diffusion (whose effects may be limited by appropriate agitation) and resistance to intraparticle diffusion. Preliminary tests showed that adopting a velocity of agitation of 210 rpm allows preventing the settling of sorbent particles, insuring the concentration of the metal (and sorbent) to be homogeneous in the reactor, and minimizing the effect of resistance to film diffusion. The uptake kinetics for the three sorbents are compared under the same experimental conditions in Fig. 3. The equilibrium time varies with the sorbent: ≈120 min for A_LPEI, ≈90 min for A_LPEI-P, and ≈60 min for A_LPEI-PQ. The increase in the density of reactive groups and the diversity in functional groups tend to enhance kinetic rate. Hubbe et al. [72,73] discussed the different experimental conditions requested for appropriately applying the pseudo-first order and pseudo-second order rate equations (Table S7a). Among the criteria that are frequently not enough taken into account they reported the variability of solute concentration in the solution. They remind that the correct interpretation of PSORE model requires the concentration remaining constant to be able to correlate mechanism interpretation (chemisorption *vs.* physisorption) with good mathematical fit of experimental profiles with the relevant equation. Hubbe et al. [72] concluded that, when the conditions are not satisfied, the PSORE fit can be more appropriately correlated to a system controlled by resistance to intra-particle diffusion. Herein, except for A_LPEI (where concentration variation does not exceed 10%), the other sorbents show large concentration

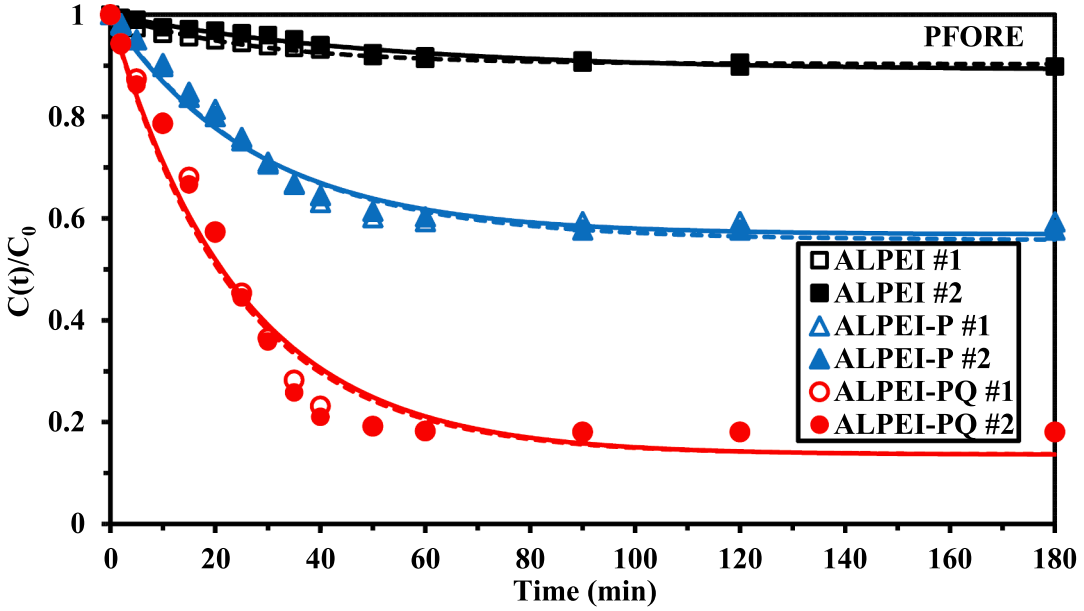


Fig. 3. W(VI) sorption using A_LPEI, A_LPEI-P, and A_LPEI-PQ at pH_0 5 – Modeling with the PFORE (C_0: 0.565 mmol W L^{-1}; SD: 0.4 g L^{-1}; v: 210 rpm; T: 22 ± 1 °C; duplicated series).

variations and the interpretation of mathematical fits must be considered just as a tool for comparing the systems. Table 1 summarizes the parameters of the models (and their statistical criteria) for the three sorbents. Globally, the kinetic profiles are best fitted by the PFORE: the calculated equilibrium sorption capacities are close to the experimental values (variation < 7.6%). Except for A_LPEI, both R^2 and AIC criteria show that the PFORE describes better W(VI) sorption. Consistently with the initial slopes of the kinetic curves (Fig. 3), the apparent rate coefficient k_1 slightly increases with sorbent quaternization (from 3.46 to 3.62 × 10^{-2} min^{-1} to 4.06–4.20 × 10^{-2} min^{-1}). It is important to remind that PFORE and PSORE have been initially designed for describing the kinetics of homogeneous chemical reaction; however, when applied to heterogeneous systems the rate parameters must be considered as apparent rates (which implicitly integrate the contribution of diffusion mechanisms). Though the RIDE is not the best equation for fitting experimental profiles (Figure S15), it may be used for comparing the systems and approaching the order of magnitude of effective diffusivity coefficient (D_e, m^2 min^{-1}) of W(VI) into the three sorbents. Table 1 reports the calculated values of D_e: a greater variation is reported for the duplicate values in the case of A_LPEI (8.2–5.2 × 10^{-9} m^2 min^{-1}) compared with the values reported for A_LPEI-P (6.1–6.8 × 10^{-9} m^2 min^{-1}). The quaternization of the sorbent leads to little decrease in the size of the beads; contrary to the trends observed in Fig. 3, D_e values are significantly decreased (i.e., 3.0–2.9 × 10^{-9} m^2 min^{-1}). Anyway, the values of D_e (i.e., 8.2–2.9 × 10^{-9} m^2 min^{-1}) are only one order of magnitude lower than the self-diffusivity of tungstate in water (i.e., 5.51 × 10^{-8} m^2 min^{-1}, [74]). This means that the resistance to intraparticle diffusion does not play a critical role in the overall control of W(VI) sorption; this is directly correlated to the large porosity of the sorbents (Section 3.1.1.). This conclusion is particularly meaningful since the size of tungstate ions in solution may be drastically increased due to the formation of polynuclear species in moderately acidic solutions ($W_{12}O_{39}^{6-}$, Figure S13).

3.2.3. *Sorption isotherms and thermodynamics*

The sorption isotherms report the distribution of the solute for different concentrations between solution and sorbent at fixed temperature and under similar pH conditions. Two important criteria can be deduced from experimental profiles: (a) the sorption capacity on the saturation plateau, and (b) the initial slope of the isotherm (which can be correlated to the affinity coefficient). Fig. 4 compares the sorption isotherms at T: 22 ± 1 °C and pH_0: 5. This figure combines the duplicates and the modeling of experimental profiles with the Sips equation; duplicate experimental curves show the good reproducibility of sorption tests (Figure S16). Figures S17 shows the fitting of cumulated duplicated series with Sips and Temkin equations. Table 2 compares the modeling of experimental curves for A_LPEI, A_LPEI-P, and A_LPEI-PQ (modeling of individual curves are reported in Table S8). For the three sorbents, the Sips equation (a combination of Langmuir and Freundlich equations) best fits sorption isotherms. In the case of A_LPEI, the calculated sorption capacity at saturation drastically exceeds the experimental value (1.071 mmol W g^{-1} *vs.* 0.459 mmol W g^{-1}. Considering N content (i.e., 3.13 mmol N g^{-1}), the molar ratio at saturation reaches 6.8 mol N per mole W (VI). Assuming that the predominant specie ($W_{12}O_{39}^{6-}$) is sorbed, the molar ratio tends to 0.57 mol N per mole of polynuclear specie; this molar ratio is not consistent with charge balance (contrary to the charge ratio: 6.8 protonated amine per $W_{12}O_{39}^{6-}$).

After the functionalization of A_LPEI (A_LPEI-P and A_LPEI-PQ), the calculated sorption capacities at equilibrium are more consistent with experimental data (overestimation by 17% for A_LPEI-P and 4% for A_LPEI-PQ). The functionalizations strongly increase sorption performances, both in terms of maximum sorption capacity (0.46 < 1.09 < 1.77 mmol W g^{-1}) and affinity coefficient (0.345 < 2.96 < 8.32 L $mmol^{-1}$), while the exponential term hardly changes (in the range 1.13–1.24). While the phosphorylation of A_LPEI maintains N-content, P content reaches 1.39 mmol P g^{-1} (as –P(=O)(O-C_4H_9)$_2$). The increase in maximum sorption capacity (i.e., 0.63 mmol W g^{-1}) represents only 45% of grafted phosphonate moieties. The stoichiometric ratio between new functional groups and tungstate approaches 2:1. Obviously, the environment of phosphonate groups with amine groups (under different configurations) and the change in acid-base properties (pH_{PZC} values) do not allow the direct comparison of sorption properties on the simple basis of addition of individual densities of reactive groups. The same features and explanation can be applied to A_LPEI-PQ sorbent. The maximum sorption capacity increases by 0.68 mmol W g^{-1}, while for constant P content, the increase in N content (as quaternary ammonium salt) reaches 2.6 mmol N g^{-1}. The molar ratio on additional quaternary ammonium and W(VI) sorption capacity tends to 3.8; meaning that the sorption mechanism does not involve a simple and single ion-exchange mechanism for the binding of polynuclear tungstate species. In order to approach the effect of multi-functionality the sorption isotherms for A_LPEI-P and A_LPEI-PQ have been tentatively fitted with the Langmuir Dual Site equation:

$$q_{eq} = \frac{q_{m,L1} C_{eq}}{1 + b_{L1} C_{eq}} + \frac{q_{m,L2} C_{eq}}{1 + b_{L2} C_{eq}} \quad (2)$$

where the parameters are similar to those reported for the Langmuir equation (Table S7b) for the two types of reactive sites (Site #1 and Site #2). Table S8 summarizes the parameters (and statistical criteria), while Figure S18 reports the modeling of the isotherms with the Langmuir Dual Site model (Table S9). In the case of A_LPEI-P, the introduction of the second reactive group does not improve the quality of the fit; the Langmuir fit remains the most appropriate. In addition, Figure S19 shows that the contribution of the Site #2 is limited to 0.125 mmol W g^{-1} (almost equally on the whole range of concentrations, and less than 12% of the maximum sorption capacity). In the case of A_LPEI-PQ, the

Table 1
W(VI) uptake kinetics using - Parameters of the models.

Model	Parameter	Unit	Sorbent					
			A_LPEI		A_LPEI-P		A_LPEI-PQ	
			#1	#2	#1	#2	#1	#2
Exper.	$q_{m,exp.}$	mmol W g^{-1}	0.142	0.145	0.571	0.603	1.146	1.158
PFORE	$q_{m,1}$	mmol W g^{-1}	0.135	0.156	0.606	0.630	1.211	1.222
	$k_1 \times 10^2$	min^{-1}	3.68	1.94	3.62	3.46	4.06	4.20
	R^2	–	0.979	0.981	0.977	0.989	0.978	0.974
	AIC	–	−154	−158	−108	−118	−83	−86
PSORE	$q_{m,2}$	mmol W g^{-1}	0.160	0.209	0.741	0.775	1.459	1.158
	$k_2 \times 10^2$	g $mmol^{-1}$ min^{-1}	27.1	7.88	5.05	4.56	3.00	3.12
	R^2	–	0.984	0.973	0.948	0.968	0.947	0.942
	AIC	–	−162	−155	−99	−105	−78	−76
RIDE	$De \times 10^9$	m^2 min^{-1}	8.19	5.19	6.76	6.07	3.02	2.88
	R^2	–	0.990	0.963	0.948	0.965	0.933	0.928
	AIC	–	−171	−148	−93	−98	−69	−68

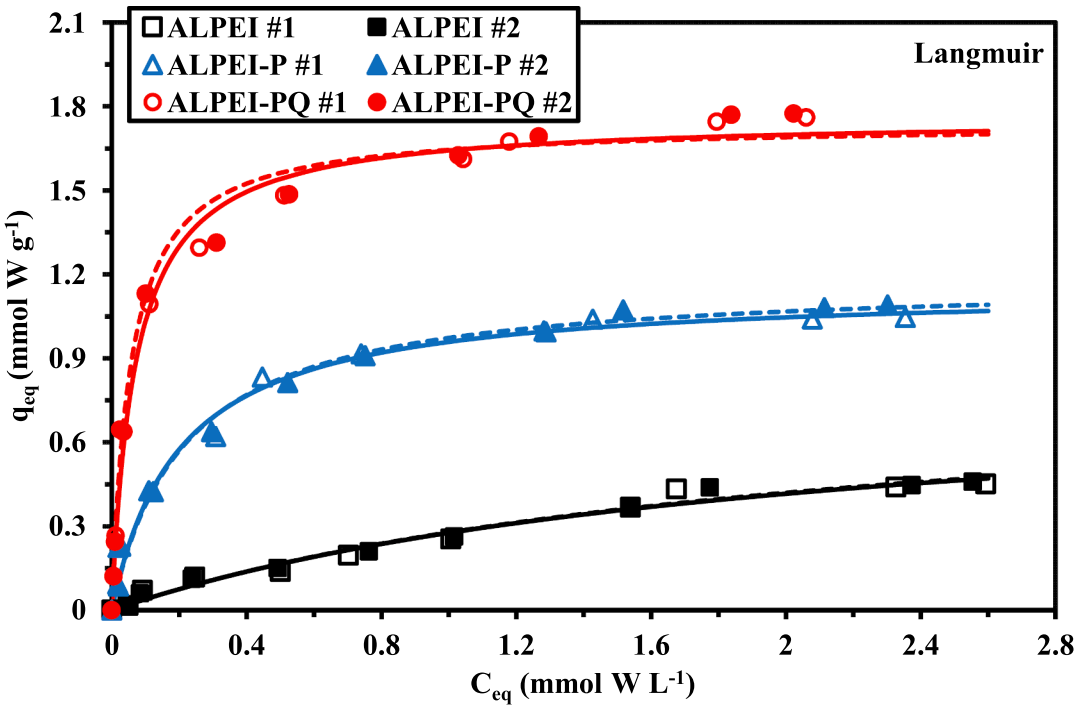


Fig. 4. W(VI) sorption isotherm at pH_0 5 using A_LPEI, A_LPEI-P, and A_LPEI-PQ – Modeling with the Langmuir equation (C_0: 0.05–2.8 mmol W L^{-1}; SD: 0.4 g L^{-1}; v: 210 rpm; T: 22 °C; time: 48 h; pH_{eq}: 5.09–5.14 for A_LPEI, 4.91–4.82 for A_LPEI-P, and 4.95–4.76 for A_LPEI-PQ; duplicated series).

Table 2
W(VI) sorption isotherms using A_LPEI, A_LPEI-P, and A_LPEI-PQ – Parameters of Langmuir, Sips and Temkin models (cumulating duplicated series).

Model	Parameter	Unit	Sorbent		
			A_LPEI	A_LPEI-P	A_LPEI-PQ
Experimental	$q_{m,exp.}$	mmol W g^{-1}	0.459	1.091	1.771
Langmuir	$q_{m,L}$	mmol W g^{-1}	0.849	1.167	1.736
	b_L	L mmol^{-1}	0.484	4.808	16.11
	R^2	–	0.982	0.989	0.990
	AIC	–	−162	−133	−115
Freundlich	k_F	mmol$^{1-1/n}$ g^{-1} L$^{1/n}$	0.265	0.892	n.s.
	n_F	–	1.569	3.146	
	R^2	–	0.979	0.959	
	AIC	–	−169	−118	
Sips	$q_{m,S}$	mmol W g^{-1}	1.071	1.276	1.839
	b_S	(mol L^{-1})^{nS}	0.345	2.956	8.320
	n_s	–	1.133	1.240	1.216
	R^2	–	0.982	0.991	0.993
	AIC	–	−170	−151	−121
Temkin	a_T	L mol^{-1}	15.47	97.45	308.4
	b_T	kJ kg mol^{-2}	21.78	12.07	8.624
	R^2	–	0.911	0.985	0.992
	AIC	–	−141	−143	−121

n.s.: non-significant.

relative contributions of the two sites vary with the temperature. More specifically, the Site #1 contributes to maximum sorption capacity in the range 1.4–1.7 mmol W g^{-1}, while the contribution of Site #2 reaches a maximum sorption capacity in the range 0.57–1.05 mmol W g^{-1}. In most cases, the affinity coefficient of Site #2 is much lower than that of Site #1. It is noteworthy that the quality of isotherm fits (with the LDS model) decreases with increasing the temperature.

The thermodynamic parameters (changes in enthalpy, ΔH^0, and Gibbs free energy, ΔH^0, in kJ mol^{-1}, and entropy change, ΔS^0, in J K^{-1} mol^{-1}) were calculated using the van't Hoff equation:

$$\ln K_{eq}^0 = \frac{-\Delta G^0}{RT} = \frac{-\Delta H^0}{RT} + \frac{\Delta S^0}{R} \quad (3)$$

where K_{eq}^0 is the standard thermodynamic equilibrium constant. Tran et al. [75] discussed the application of a series of sorption isotherms with their relevant thermodynamic approach. They reported the importance of converting the parameters of equilibrium constant (K_{model}, for example affinity constant in the case of Langmuir equation) to dimensionless form. In addition, they listed the relationship between K^0_{eq} and K_{model}.

In the case of the Langmuir equation, the relationship reduces to:

$$K_{eq}^0 = b_L^* \times \frac{C^0_{sorbate}}{\gamma_{sorbate}} \quad (4)$$

where b_L* is the converted form of the Langmuir affinity coefficient (dimensionless), $C^0_{sorbate}$ is the unitary standard concentration of the sorbate (~1 mol L^{-1}), and $\gamma_{sorbate}$ is the activity coefficient of the sorbate (~1, for diluted solution).

Fig. 5 reports W(VI) sorption isotherms at different temperatures, with the Langmuir and the Sips fits (Table 3). Both maximum sorption capacity and affinity coefficient (correlated to the initial slope) increase with the temperature. The sorption of W(VI) is endothermic for A_LPEI-PQ sorbent. Figure S20 shows the corresponding van't Hoff plot applied to the affinity coefficient from Langmuir equation (the relevant parameters for duplicated series are all joined). The dispersion of data leads to poor determination coefficient; the thermodynamic parameters reported in Table S10 must be considered as indicative values. The enthalpy change is positive meaning that sorption is endothermic and relatively low (≈ 2.1 kJ mol^{-1}), while the entropy changes is close to 150 J K^{-1} mol^{-1}. The positive entropy means that with W(VI) sorption the randomness of the system increases. This increase in the entropy of the global systems is associated with the dehydration of metal ions and the release of exchanged ions. The negative value of the change of Gibbs free energy means that the sorption process is spontaneous (and becomes more spontaneous with thermal activation).

Table 4 compares the sorption properties of a series of sorbents for W

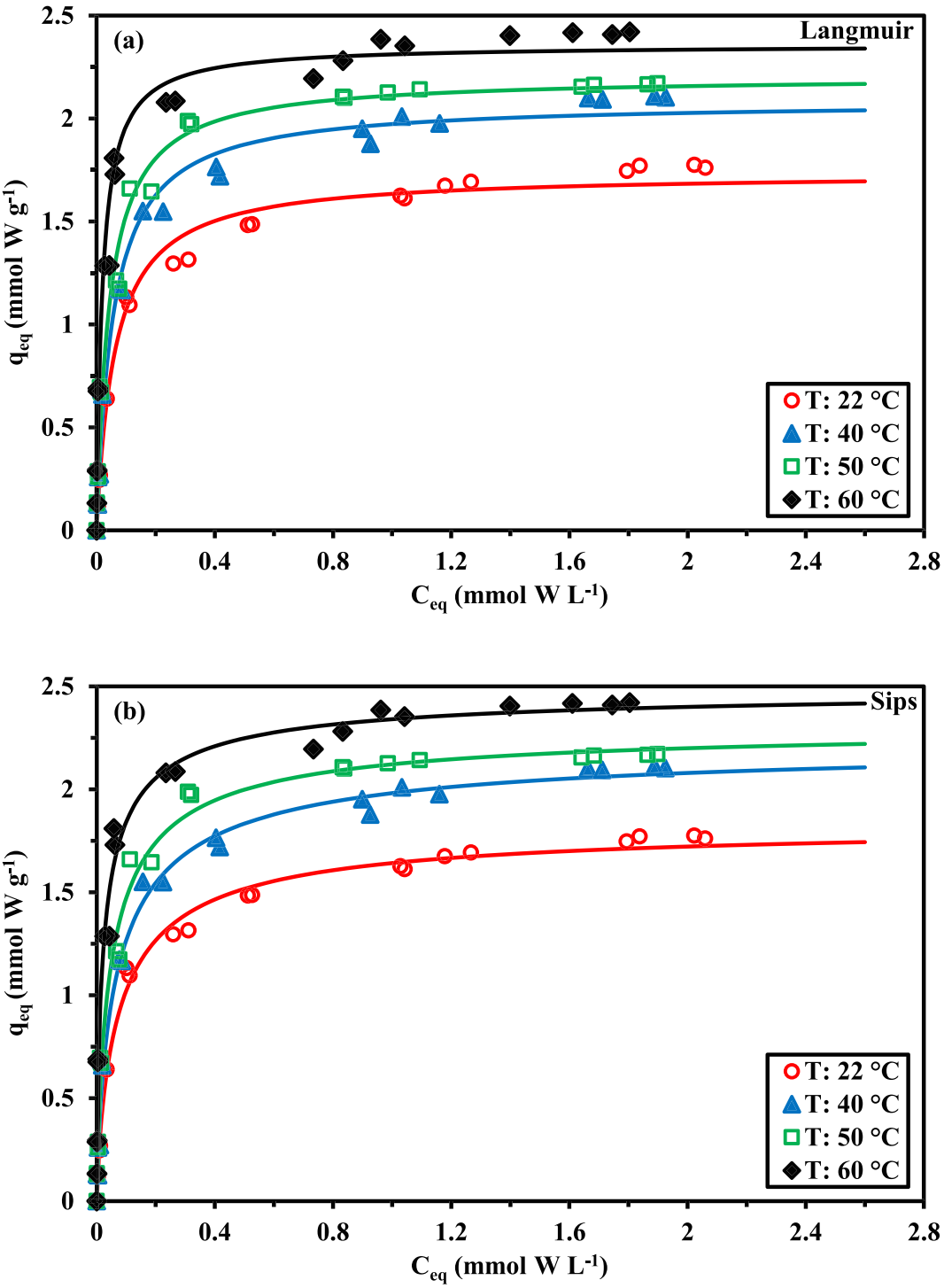


Fig. 5. Effect of temperature on W(VI) sorption isotherm at pH_0 5 using A_LPEI-PQ – Modeling with the Langmuir equation (a) and the Sips equation (b) (C_0: 0.05–2.8 mmol W L^{-1}; SD: 0.4 g L^{-1}; v: 210 rpm; time: 48 h; duplicated series – modeling with cumulated series).

(VI). Taking into account the Langmuir-related parameters and the equilibrium contact time, A_LPEI-PQ is part of the most efficient sorbents, comparable to acid-treated carbon cloth [76]; just surpassed by alumina [18]. Most of these sorbents have been tested in the pH range 4–7. In strong acid solutions, the sorption capacities are negligible; except for TVEX-TOPO resin (a resin impregnated with trioctylphosphine oxide) that accommodates 0.5 M HNO_3 solutions.

3.2.4. Binding mechanisms

The FTIR analysis of sorbents before and after metal sorption confirms suspected binding mechanisms. In the case of A_LPEI, the poor sorption levels hardly alter FTIR spectrum: the most significant change is observed in the region where protonated amine groups are identified (i.e., 1530–1300 cm^{-1}), meaning that protonated amine groups bind tungstate anions (Figure S4, Table S2). The sorption of W(VI) onto phosphorylated A_LPEI beads is followed by a significant decrease of the relative intensity of the typical bands of phosphonate groups, while after metal desorption the peaks are restored: as expected, phosphonate groups are involved in tungstate binding. For bi-functionalized sorbent (i.e., A_LPEI-PQ), the sorption of tungstate induces numerous additional

Table 3
Effect of temperature on W(VI) sorption isotherms for A_LPEI-PQ – Parameters of Langmuir, Sips and Temkin models (cumulating duplicated series).

Model	Parameter	Unit	Temperature (°C)			
			22	40	50	60
Experimental	$q_{m,exp.}$	mmol W g^{-1}	1.771	2.108	2.170	2.421
Langmuir	$q_{m,L}$	mmol W g^{-1}	1.736	2.084	2.206	2.358
	b_L	L $mmol^{-1}$	16.11	17.81	22.64	49.58
	R^2	–	0.990	0.989	0.990	0.984
	AIC	–	−115	−104	−102	−86
Sips	$q_{m,S}$	mmol W g^{-1}	1.839	2.235	2.316	2.499
	b_S	$(mol\ L^{-1})^{nS}$	8.320	7.826	10.98	14.81
	n_s	–	1.216	1.289	1.254	1.385
	R^2	–	0.993	0.993	0.993	0.991
	AIC	–	−121	−118	−124	−109
Temkin	a_T	L mol^{-1}	308.4	494.4	840.3	1909
	b_T	kJ kg mol^{-2}	8.624	8.256	8.597	8.848
	R^2	–	0.992	0.986	0.978	0.983
	AIC	–	−121	−106	−89	−86

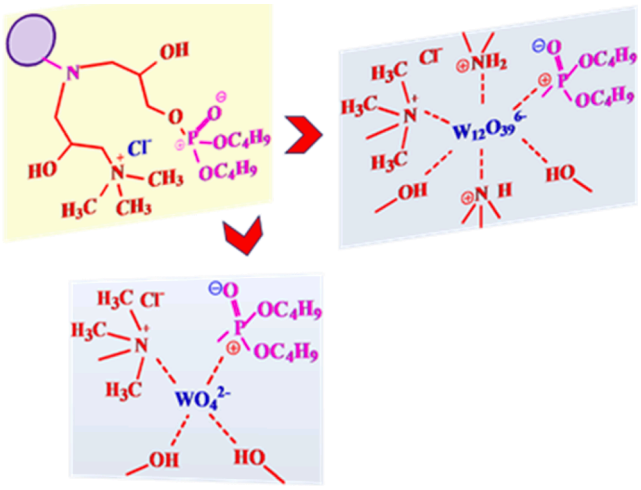
Table 4
Comparison of tungstate sorption properties for selected sorbents.

Sorbent	pH	Time	$q_{m,exp.}$	$q_{m,L}$	b_L	Ref.
Alumina	4	–	2.0	2.1	540	[18]
Acid-treated carbon-cloth	7	30	1.35	1.99	0.670	[76]
Composite soil	5	6000	–	0.011	0.035	[21]
Kaolinite	5	2880	0.04	0.036	0.0035	[20]
Diamino resin	6	60	0.344	0.369	3.13	[80]
Nanocrystalline iowaite	≈6	480	–	0.294	32.2	[19]
Multi-walled carbon nanotubes	6	120	0.096	0.112	17,292	[27]
Soil	4.7	1080	0.027	0.035	0.259	[23]
TVEX-TOPO resin	0.5 M HNO_3	75	–	0.194	6.43	[33]
A_LPEI	5	60	0.459	0.849	0.484	*This work*
A_LPEI-P	5	60	1.09	1.17	4.81	*This work*
A_LPEI-PQ	5	60	1.77	1.74	16.11	*This work*

Units: Time (min); q_m: mmol W g^{-1}; b_L: L $mmol^{-1}$.

changes to those observed for A_LPEI-P (assigned to phosphonate moieties), such as the disappearance of the quaternary ammonium salt peak (at 974 cm^{-1}), the superposition of W-O stretching with the P-O stretching (at 1251 cm^{-1}), and the appearance of a shoulder at 1730 cm^{-1} (attributed to carboxylic acid groups). Contrary to A_LPEI-P, in the case of A_LPEI-PQ metal desorption does not completely restore the FTIR spectrum. However, despite these chemical modifications the sorption/desorption performances are still maintained for a minimum of five cycles (see Section 3.2.6.). These conclusions are confirmed by the substantial changes observed in the XPS spectra of A_LPEI and A_LPEI-PQ (reported in Figures S6-S7 and Table S5): amine groups (protonated form) are involved in W(VI) binding for A_LPEI, while metal binding affects amine-based groups (not only quaternary ammonium salt sites), and O-based groups (from phosphonate moieties). In addition, the analysis of W 4f signal apparently shows that a small fraction of tungstate is reduced to W(V) for both A_LPEI and A_LPEI-PQ sorbents.

This information combined with the effect of pH on metal sorption (protonation/deprotonation of reactive groups in relation with both overall charge surface and pH_{PZC}, and metal speciation) allows proposing different sorption mechanisms for the binding of tungstate anions onto A_LPEI-PQ sorbent (Scheme 2). The reactive groups that may significantly contribute to metal binding are hydroxyl, amine groups (present on quaternary ammonium moiety), and phosphonate chelating groups. These hypotheses are supported by the study of the effect of pH



Scheme 2. Tentative mechanisms for the sorption of tungstate anions onto A_LPEI-PQ.

and the evaluation of pH_{PZC} values (electrostatic attraction and ion-exchange process depends on the pH). At optimum pH value, the partial protonation of reactive groups and the presence of quaternary ammonium groups support the anion exchange mechanism between R_4N^+ groups and tungstate anions (including polynuclear species: $W_XO_Y^{Z-}$). On the other hand, phosphonate groups may contribute to chelate tungstate through electron-donating groups (in addition to hydroxyl and nitrogen from free amine groups, depending on the pH). These different modes of interactions can be correlated to the optimum pH values, the comparison of FTIR and XPS spectra. The combination of ion-exchange and chelating modes for the different reactive groups enhances the binding of mononuclear or polynuclear species; their respective contributions depend on the pH (metal speciation and the extent of protonation and deprotonation of reactive groups).

3.2.5. *Effect of competitor metal ions – Selectivity*

In order to anticipate on the possibility to use A_LPEI-PQ for the treatment of complex solutions, the sorption properties of W(VI) have been explored in multi-component equimolar solutions containing Ca (II), Mg(II), Fe(III), Al(III), Zn(II), and Nd(III) (metal ions usually found in the leachates of W-bearing Egyptian ores). Different pH values (from 3 to 6) have been tested.

Fig. 6a shows that the selectivity for W(VI) increases with decreasing the pH; this conclusion is confirmed by the semi-quantitative EDX analysis of sorbent surface (Figure S21). The sorption of metal cations increases with pH, contrary to tungstate anions. It is noteworthy that the presence of competitor ions reverse the effect of the pH on the distribution ratio (Figure S22): D_w increases with the pH in single-component solutions, contrary to multi-component solutions. This inversion is probably associated with the increasing competitor effect of other metal ions when increasing the pH; though W(VI) sorption is less favorable in acidic solutions, the competition of metal cations at higher pH values limits the number of reactive groups available for W(VI) binding. Fig. 6a clearly confirms the highest affinity of the sorbent for W(VI) at pH_{eq} 3.4. The selectivity for W(VI) against metal cations follows the trend:

Mg(II) (31.9) > Ca(II) (17.8) > Al(III) (15.1) > Zn(II) (9.3) > Fe(III) (8.4) > Nd(III) (5.3).

Tungsten is part of the hard acids according the hard and soft acidic and base theory [77], as most of the competitor metals (except Zn(II)). Since a significant part of tungstate binding occurs through ion-exchange mechanisms on quaternary ammonium salt moieties, the preference of the sorbent for metal anions can explain its good selectivity for tungstate (or other metal-anion forming species). The weaker selectivity for Nd, its high-value, and presence in Egyptian ores from

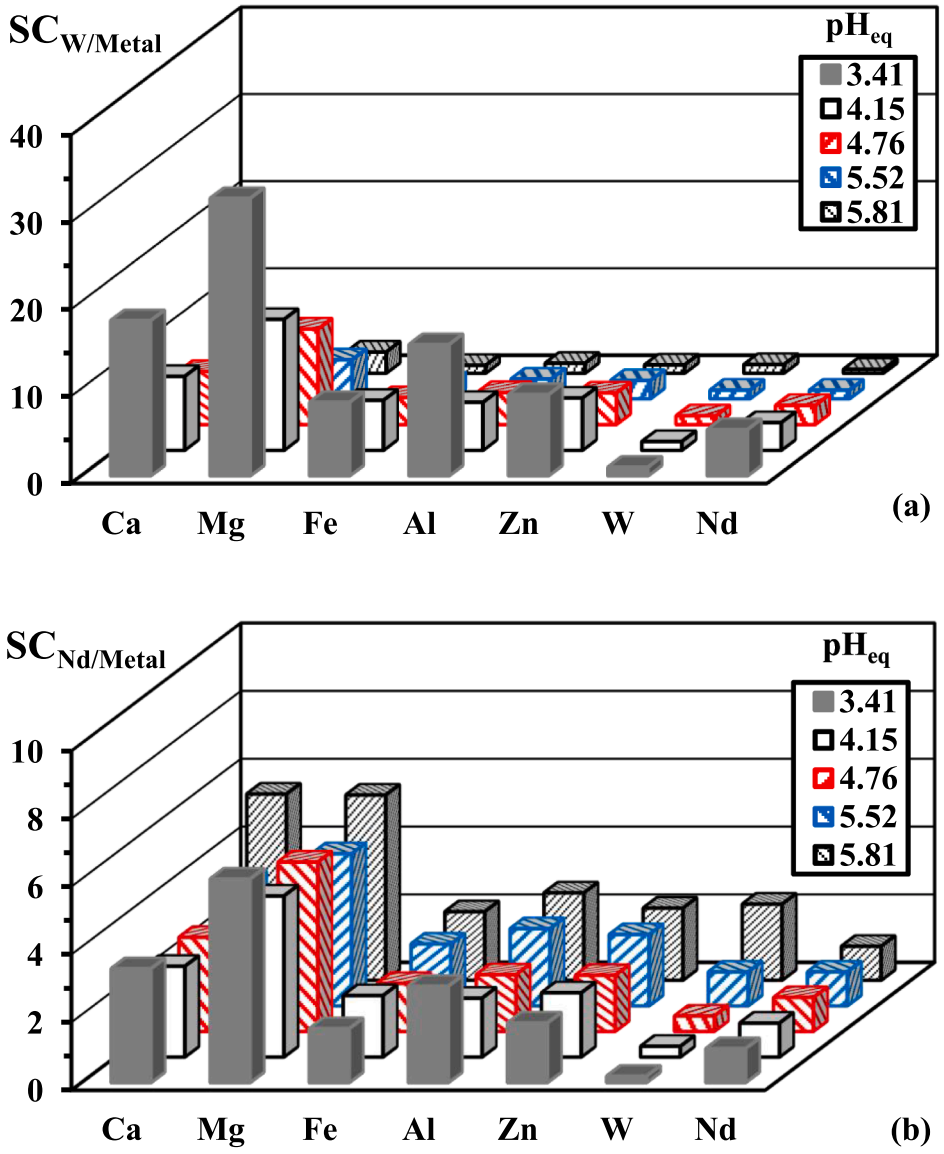


Fig. 6. Effect of pH on sorption selectivity using A_LPEI-PQ: (a) $SC_{W/Metal}$, and (b) $SC_{Nd/Metal}$ (equimolar concentrations, C_0: 1 mmol L^{-1}; SD: 1 g L^{-1}; time: 600 min; v: 210 rpm; T: 22 °C).

Eastern Desert made pertinent the supplementary analysis of selectivity profiles for Nd(III) against other metal anions. Fig. 6b shows that the selectivity of A_LPEI-PQ for Nd(III) is hardly affected by the pH (though little better at pH 5.8):

Mg(II) (5.5) ≈ Ca(II) (5.5) > Al(III) (2.6) > W(VI)≈Zn(II)≈Fe(III) (2.3–2.0).

The selectivity for Nd(III) depends on the pH only for Ca(II) (increasing from 2.7 to 5.5).

Figure S23 reports the cumulative sorption capacity that increases with the pH to reach a maximum (close to 3.1 mmol g^{-1}) at pH 5.5–5.8. The relative fraction of W(VI) in the sorbent progressively decreases with the pH (from 38% to 15%), while that of Nd(III) remains stable (around 18%) below pH 4.8, before slightly increasing up to 22% at pH 5.8. The fractions of the other metal ions in the sorbent are poorly affected by the pH:

Fe(III) (15.2 ± 1.5 %) > Zn(II)≈Al(III) (12.7 ± 2.3 %) > Ca(II) (8.1 ± 0.9 %) > Mg(II) (6.4 ± 1.5 %).

In acidic solutions, the sorbent selectively recovers W(VI) over metal cations; increasing the pH to 5.8 (after tungstate removal) would not allow separating neodymium from residual metals but could contribute to enriching the concentration the rare earth element in the sorbent.

3.2.6. *Metal desorption and sorbent recycling*

The evaluation of a sorbent requires investigating desorption of metal-loaded material, not only for recovering toxic or valuable metal but also for analyzing the possibility to recycle the sorbent. Metal desorption is highly effective using 0.2 M NH_4Cl solution (Figure S24). Tungstate is fully desorbed within 30 min of contact. The same eluent can be used indifferently with A_LPEI, A_LPEI-P, and A_LPEI-PQ, without significant differences in the kinetic profiles. Five cycles of sorption and desorption were tested for evaluating the variation in both sorption efficiency and desorption yield. The FTIR analysis of the sorbents after these five cycles has shown significant changes compared with their original spectra. Therefore, the comparison of sorption and desorption performances is of critical importance. Table 5 shows that the sorption efficiency progressively decreases with the number of re-uses. Since desorption efficiency is not significantly changed during the re-uses, the loss in sorption is not associated with the progressive saturation of sorption sites. Therefore, the decrease in sorption performance is probably due to the physical or chemical degradation of the sorbents.

Table 5
Metal sorption and sorbent recycling – Sorption (SE, %) and desorption (DE, %) efficiencies for five successive cycles for A_LPEI, A_LPEI-P, and A_LPEI-PQ.

Sorbent	A_LPEI		A_LPEI-P		A_LPEI-PQ	
Run	SE	DE	SE	DE	SE	DE
#1	10.5 ± 0.1	98.4 ± 2.3	45.5 ± 0.2	99.8 ± 0.9	80.3 ± 0.2	100.3 ± 0.3
#2	9.8 ± 0.1	100.4 ± 0.4	44.8 ± 0.6	100.5 ± 0.6	79.2 ± 0.1	100.3 ± 0.4
#3	9.6 ± 0.0	100.6 ± 0.2	43.9 ± 0.3	101.1 ± 0.9	78.2 ± 0.1	100.4 ± 0.5
#4	9.2 ± 0.4	100.0 ± 0.1	42.6 ± 0.2	100.7 ± 0.2	77.3 ± 0.2	99.9 ± 0.4
#5	8.7 ± 0.1	99.8 ± 0.2	41.0 ± 0.0	100.4 ± 0.6	80.3 ± 0.4	100.0 ± 0.2
Loss at 5th/ 1st (%)	17.1		10.1		5.4	

XPS analyses have shown a weak but detectable reduction of W(VI) to W (V); corollary to this reduction of the metal, the sorbent is probably partially oxidized (consistently with observed FTIR changes). It is noteworthy that the loss in sorption performance (between first and fifth cycle) significantly decreases with the functionalization of the sorbent: 17% for A_LPEI, 10% for A_LPEI-P, and down to 6% for A_LPEI-PQ. The bi-functional sorbent is remarkably stable in terms of re-use. In the case of A_LPEI, W(VI) desorption process should be improved. Masry et al. [33] successfully desorbed tungstate in the presence of ascorbic acid in the case of extractant-impregnated resins.

3.3. Application to real effluent

3.3.1. Ore pre-treatment (ore concentrate, leaching, and solvent extraction processing)

Annex A provides information on the location of ore collection (with geochemical and mineralogical relevant characteristics). The ore was pre-treated with density and magnetic concentration. The concentrate is essentially constituted of hubnerite (manganese tungstate that may contain traces of other metal tungstates). Table A1 reports the composition of the concentrate. The acidic leaching of the concentrate allows recovering 95% of manganese and 99% of iron without removing valuable elements such as W (less than 0.1%) and Nb (negligible); the composition of the acidic leachate is reported in Table A2 (XRF characterization of produced tungstic acid). The next step in the process consisted in the alkaline leaching of the tungstic acid. This step allows releasing about 99% of W(VI) and only 10% of Nb(V). The residue is washed with water and the aqueous phase is mixed with the alkaline leachate to produce the pregnant alkaline sodium tungstate solution (PLS, 1 L, pH 12.3). The composition of PLS is reported in Table A3.

The treatment of PLS (pH adjusted to 8 with HCl solution) is processed using solvent extraction (Alamine 336 in kerosene, with octanol as the modifier) [78,79]. Tungstate extraction yields 94%. Organic phase is scrubbed with demineralized water for removing sodium and silica impurities. The W-loaded organic phase is stripped with ammonium hydroxide; stripping yields 97.9%. The strip solution is evaporated to produce pure ammonium paratungstate (grade: 99.97%; with a rate of 90%). Calcination at 750 °C allows producing pure tungsten oxide (i.e., WO_3). The composition of the raffinate (i.e., residue of solvent extraction completed with scrub solution) is reported in Table A4: tungstate is one of the major elements, with concentration as high as 374.9 mg W L^{-1} (i.e., 2.04 mmol W L^{-1}), apart Na at 5.58 g Na L^{-1} (i.e., 0.243 mol Na L^{-1}).

Note: The experimental conditions, for each individual step, are fully reported in Annex A.

3.3.2. Tungstate recovery from raffinate

Consistently with the methodology followed for the study of selectivity, the raffinate was adjusted to different pH values in the range 3.3–6.3, before processing to sorption tests. Under selected experimental conditions (i.e., more specifically, SD: 1 g L^{-1}), the sorption process allows recovering almost 96% of tungstate at pH_{eq} 4.74 (optimum pH for sorption efficiency, Fig. 7a), while for other metals the recovery does not exceed 58%. The maximum sorption efficiency for the other metals is generally obtained at pH_{eq} 5.85–6.28, consistently with the trends observed in the study of selectivity (Section 3.2.5.). The curve for Na(I) is not reported; the weak removal (lower than 3%) is explained by the huge level of sodium in the raffinate. Figure S25 reports the distribution ratios (log_{10} plot) against equilibrium pH. This figure confirms these trends: (a) in most cases, the distribution ratios are poorly influenced by the pH (except for tungstate), (b) all the elements are grouped (except sodium, which large excess leads to poor concentration effect into the sorbent), and (c) tungstate uptake shows a maximum in the distribution ratio at pH_{eq} 4.74, about one order of magnitude greater in D value compared with those of other metals.

Fig. 7b plots the $SC_{W/metal}$ values *vs.* pH_{eq}. As expected (from Figure S25), the highest values for tungstate selectivity are obtained at pH_{eq} 4.74. The sorbent allows outstanding separation (selective recovery) for W(VI) against:

Na(I) (927) > Si(IV) (47.7) > Ti(IV) (42.8) > Ca(II) (35.2) > Al(III) (33.2) > Ta(V) (28.7) > Nb(V) (15.9).

Despite the complexity of the raffinate with huge excess of Na(I) and the presence of other metal cations, A_LPEI-PQ allows recovering W(VI) with high efficiency at pH_{eq} close to 4.7. Under these conditions, Figure S26a reports the percentage of metals on loaded sorbent. Consistently with the huge excess of Na(I) in the raffinate, this element represents about 56 % of the metals bound to A_LPEI-PQ. Similarly, W(VI) represents about 19%, Si(IV) about 13.5% and Al(III) ≈5.5%; other elements count for less than 6%. Figure S26b gives another visualization of these data through the plot of the concentration factor (CF: q_{eq}/C_0, L g^{-1}). The concentration effect is significantly higher for the metals that form anionic complexes (such as tungstate, niobiate). Apart the direct effect of their relative concentration in the raffinate, the strong affinity of A_LPEI-PQ for metal ions that form anionic complexes makes it highly selective for tungstate, with a good concentration effect, suitable for valorization of the metal from the residues of solvent extraction processing. Figure S27 reports the semi-quantitative EDX analysis of the sorbent after treating the raffinate at pH_{eq} 3.28 and 6.28. These analyses clearly show the wide spectrum of metal bounds to A_LPEI-PQ. It is especially interesting to observe the affinity of the sorbent for strategic metals such as niobium, tantalum, titanium or nickel.

3.3.3. Cost analysis and comparison of performance with commercial resins

The cost analysis of A_LPEI-PQ synthesis is made difficult by the lab-scale production: cost of reagents, operating costs, investment amortization would considerably change with a large-scale application. In Supplementary Information (Annex B), a very simple evaluation of the production costs (only based on the compilation of reagent expenses) is provided. The sorption capacity of A_LPEI-PQ is compared for tungstate recovery from the residues of solvent extraction (in the processing of ore leachate) with the performances obtained with two commercial resins (i.e., Amberlite IRA402 and Dowex 1X8 200–400 Mesh). Under comparable experimental conditions, the sorption capacities of A_LPEI-PQ reaches 0.487 mmol W g^{-1}; meaning significantly higher than those obtained with Amberlite IRA402 (i.e., 0.070 mmol W g^{-1}), or Dowex 1X8 (i.e., 0.145 mmol W g^{-1}). Referred to the uptake of 1 mmol W, the cost of material in metal recovery is significantly lower for the new sorbent (i.e., 75 €) than for commercial resins (i.e., 156–193 €). Obviously, the incomplete evaluation of the production cost for A_LPEI-PQ requires considering with caution this analysis; however, this pre-evaluation confirms that the new sorbent offers promising perspectives.

4. Conclusion

The poor efficiency of A_LPEI sorbent for binding tungstate from

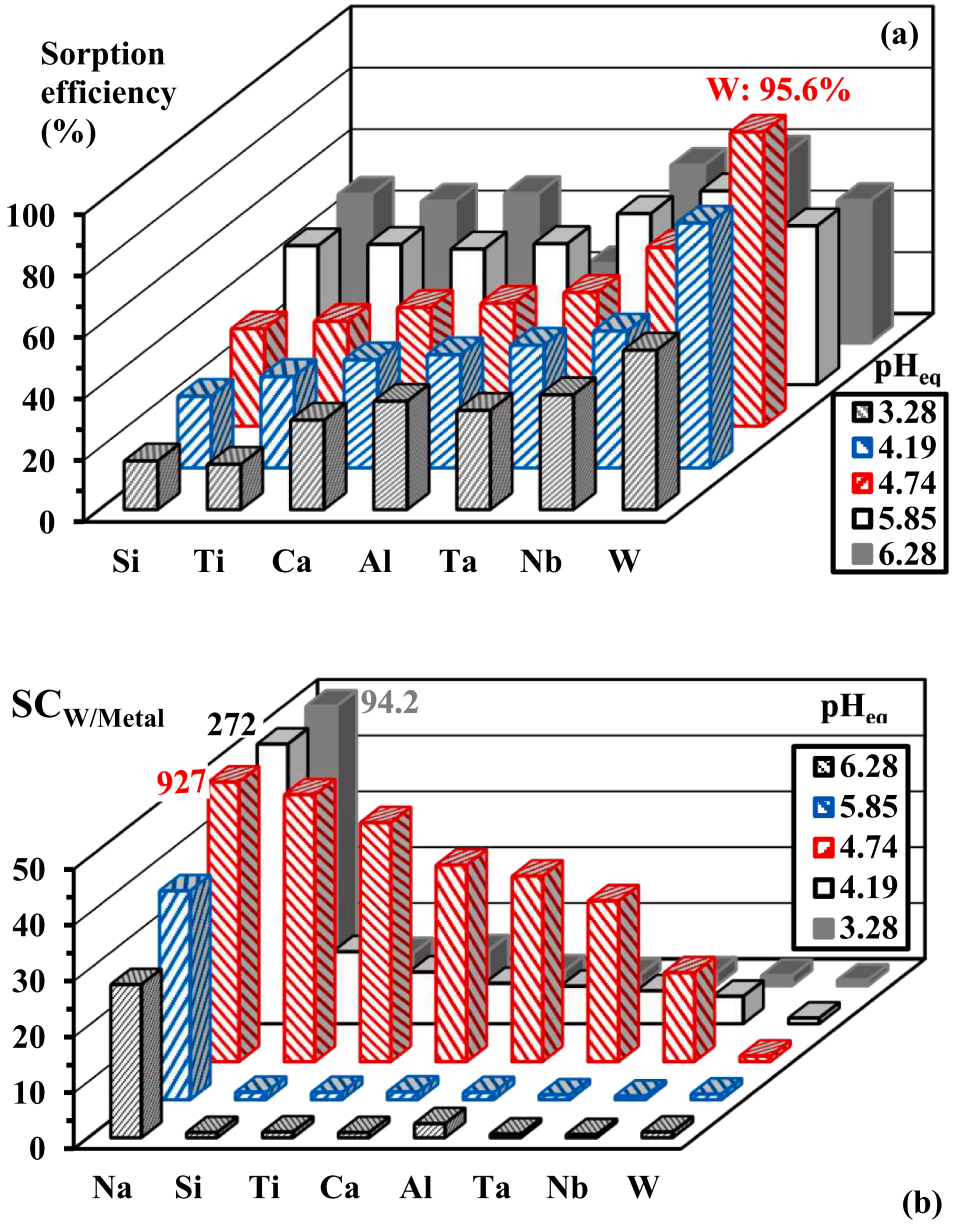


Fig. 7. Effect of the pH on sorption efficiency (%) and selectivity coefficient $SC_{W/Metal}$ (b) for A_LPEI-PQ used for the recovery of W(VI) from raffinate produced during the treatment of hubnerite leachates (SD: 1 g L^{-1}; T: 22 ± 1 °C; v: 210 rpm; time: 10 h; numbers represent outstanding out-of-range SC values for pH_{eq} 3.28–4.74).

weakly acidic solutions was incentive to functionalize the support using phosphorylation. Despite the benefit of phosphonate grafting that increases the maximum sorption capacity by ≈0.6 mmol W g^{-1}, the subsequent quaternization of the modified sorbent allows increasing even more the sorption capacity (by 0.68 mmol W g^{-1} for A_LPEI-PQ). The study of pH effect also compared the behavior with directly quaternized A_LPEI beads; these results show that the synergistic effect of quaternary ammonium groups and phosphonate moieties benefits to W(VI) sorption performance as a justification of bi-functionalization. With a maximum sorption capacity close to 1.77 mmol W g^{-1}, the bi-functional sorbent is part of the most efficient sorbents reported in the literature. Both, the strong affinity of quaternary ammonium salt and phosphonate groups and the large meso-porosity of the material explain the fast uptake (equilibrium reached within 60 min). The synergistic effects of phosphonate and quaternary ammonium salt groups strongly enhance sorption isotherms and uptake kinetics. The sorption of tungstate involves both complexation (with phosphonate groups) and ion-exchange with quaternary ammonium groups. The sorption isotherms can be fitted using the Sips equation and the Langmuir Dual Site model, while the uptake kinetics are efficiently described by the pseudo-first order rate equation. XPS and FTIR spectrometric analyses confirm the chemical modification of the sorbent and contribute to explain the interaction mechanisms. Despite the non-reversible modification of the sorbents during sorption/desorption cycles and the partial reduction of tungstate on the sorbents, the sorption properties remain remarkably stable (especially for the bi-functional sorbent). Ammonium chloride solution (0.2 M) allows achieving the complete desorption of tungstate at a relatively fast rate (less than 30 min of contact). The bi-functional sorbent shows remarkable selectivity for tungstate in multi-component solutions (synthetic equimolar solutions). This is also confirmed by the efficient recovery of the metal from the raffinate produced during W(VI) solvent extraction from the leachates of hubnerite concentrate (in the processing of Egyptian ores from Southwestern Desert).

CRediT authorship contribution statement

Mohammed F. Hamza: Conceptualization, Methodology, Software, Formal analysis, Writing – review & editing. **Khalid A.M. Salih:** Methodology, Software, Formal analysis, Resources. **Kanggen Zhou:** Methodology, Software, Resources. **Yuezhou Wei:** Conceptualization, Methodology, Project administration, Funding acquisition. **Hanaa A. Abu Khoziem:** Methodology, Formal analysis, Investigation, Data curation. **Saad H. Alotaibi:** Data curation, Project administration, Funding acquisition. **Eric Guibal:** Conceptualization, Methodology, Data curation, Investigation, Software, Writing – review & editing.

Declaration of Competing Interest

The authors declare that they have no known competing financial interests or personal relationships that could have appeared to influence the work reported in this paper.

Acknowledgements

S. H. Alotaibi acknowledges Taif University for Researchers Supporting Project (TURSP- 2020/83), Taif University, Saudi Arabia. W.Y acknowledges the support of National Natural Science Foundation of China [U1967218, and 11975082]. E. Guibal, and M. F Hamza acknowledge the support of IMHOTEP Program (MetalValor project).

Appendix A. Supplementary material

Supplementary data to this article can be found online at https://doi.org/10.1016/j.seppur.2022.120893.

References

[1] RSC, Periodic Table, in: RSC (Ed.), RSC, London (UK), 2020.
[2] T. Welz, R. Hischier, L.M. Hilty, Environmental impacts of lighting technologies - Life cycle assessment and sensitivity analysis, Environ. Impact Assess. Rev. 31 (2011) 334–343, https://doi.org/10.1016/j.eiar.2010.08.004.
[3] D. Mishra, S. Sinha, K.K. Sahu, A. Agrawal, R. Kumar, Recycling of secondary tungsten resources, Trans. Indian Inst. Met. 70 (2017) 479–485, https://doi.org/10.1007/s12666-016-1003-8.
[4] A. Shemi, A. Magumise, S. Ndlovu, N. Sacks, Recycling of tungsten carbide scrap metal: a review of recycling methods and future prospects, Miner. Eng. 122 (2018) 195–205, https://doi.org/10.1016/j.mineng.2018.03.036.
[5] A.H. Tkaczyk, A. Bartl, A. Amato, V. Lapkovskis, M. Petranikova, Sustainability evaluation of essential critical raw materials: cobalt, niobium, tungsten and rare earth elements, J. Phys. D: Appl. Phys. 51 (2018), 203001, https://doi.org/10.1088/1361-6463/aaba99.
[6] B. Zeiler, A. Bartl, W.-D. Schubert, Recycling of tungsten: current share, economic limitations, technologies and future potential, Int. J. Refract. Met. Hard Mater. 98 (2021), 105546, https://doi.org/10.1016/j.ijrmhm.2021.105546.
[7] W.-J. Zhang, J.-H. Yang, Z.-W. Zhao, W.-Q. Wang, J.-T. Li, Coordination leaching of tungsten from scheelite concentrate with phosphorus in nitric acid, J. Centr. South Univ. 23 (2016) 1312–1317, https://doi.org/10.1007/s11771-016-3181-2.
[8] X. Chen, Z. Tan, Y. Wu, Q. Zhang, D. Pan, Eco-friendly H_2O_2 leaching for noble-metals Re and W selective recovery from waste thermoelectric materials, Therm. Sci. Eng. Prog. 19 (2020), 100563, https://doi.org/10.1016/j.tsep.2020.100563.
[9] S.B. Dimitrijevic, S.R. Velickovic, A.T. Ivanovic, F.M. Veljkovic, M.M. Jovanovic, Z. Kamberovic, S.P. Dimitrijevic, Recovery of tungsten trioxide from waste diamond core drilling crowns by nitric acid leaching, Int. J. Refract. Met. Hard Mater. 101 (2021), 105695, https://doi.org/10.1016/j.ijrmhm.2021.105695.
[10] L. Shen, X. Li, D. Lindberg, P. Taskinen, Tungsten extractive metallurgy: a review of processes and their challenges for sustainability, Miner. Eng. 142 (2019), 105934, https://doi.org/10.1016/j.mineng.2019.105934.
[11] H. Liu, H. Liu, C. Nie, J. Zhang, B.-M. Steenari, C. Ekberg, Comprehensive treatments of tungsten slags in China: a critical review, J. Environ. Manage. 270 (2020), 110927, https://doi.org/10.1016/j.jenvman.2020.110927.
[12] K.A. Won, E.C. Lee, Extraction of tungsten from acetic tungstate complex solutions by liquid membrane, Sep. Sci. Technol. 38 (2003) 1399–1415, https://doi.org/10.1081/ss-120018816.
[13] Z. Li, G.-Q. Zhang, W. Guan, L. Zeng, L. Xiao, Q.-G. Li, Z.-Y. Cao, X. Lu, Separation of tungsten from molybdate using solvent extraction with primary amine N1923, Hydrometallurgy 175 (2018) 203–207.
[14] Y. Sasaki, Various metal extraction from hydrochloric acid into n-dodecane by methylimino-dioctylacetamide (MIDOA), Sep. Sci. Technol. 55 (2020) 708–715, https://doi.org/10.1080/01496395.2019.1574831.
[15] Y. Yang, B. Xie, R. Wang, S. Xu, J. Wang, Z. Xu, Extraction and separation of tungsten from acidic high-phosphorus solution, Hydrometallurgy 164 (2016) 97–102, https://doi.org/10.1016/j.hydromet.2016.05.018.
[16] G. Zhang, W. Guan, L. Xiao, Q. Zhang, A novel process for tungsten hydrometallurgy based on direct solvent extraction in alkaline medium, Hydrometallurgy 165 (2016) 233–237, https://doi.org/10.1016/j.hydromet.2016.04.001.
[17] N. Papaiconomou, S. Viboud, Extraction of polyoxometallate anions containing tungsten towards ionic liquids, J. Solution Chem. 47 (2018) 1339–1350, https://doi.org/10.1007/s10953-018-0796-y.
[18] J.L. Vucina, D.M. Lukic, S.K. Milonjic, M.M. Stoiljkovic, Sorption of tungsten on alumina in dynamic conditions, J. Radioanal. Nucl. Chem. 267 (2005) 67–72, https://doi.org/10.1007/s10967-006-0010-3.
[19] Y. Cao, Q. Guo, Z. Shu, C. Jiao, L. Luo, W. Guo, Q. Zhao, Z. Yin, Tungstate removal from aqueous solution by nanocrystalline iowaite: an iron-bearing layered double hydroxide, Environ. Pollut 247 (2019) 118–127, https://doi.org/10.1016/j.envpol.2019.01.021.
[20] R. Li, C. Lin, X. Liu, Adsorption of tungstate on kaolinite: adsorption models and kinetics, RSC Adv. 6 (2016) 19872–19877, https://doi.org/10.1039/C5RA24201K.
[21] R. Li, R. Luan, C. Lin, D. Jiao, B. Guo, Tungstate adsorption onto oxisols in the vicinity of the world's largest and longest-operating tungsten mine in China, RSC Adv. 4 (2014) 63875–63881, https://doi.org/10.1039/c4ra09940k.
[22] R. Li, Y. Tang, X. Li, C. Tang, Y. Zhu, S. Wang, C. Lin, Adsorption behavior of tungstate on montmorillonite as a function of pH, ionic strength and competitive anion, Desalin. Water Treat. 150 (2019) 274–281, https://doi.org/10.5004/dwt.2019.23728.
[23] G. Petruzzelli, F. Pedron, Adsorption, desorption and bioavailability of tungstate in Mediterranean soils, Soil Syst. 4 (2020) 53, https://doi.org/10.3390/soilsystems4030053.
[24] G. Sen Tuna, W. Braida, Evaluation of the adsorption of mono- and polytungstates onto different types of clay minerals and pahokee peat, Soil Sediment Contam. 23 (2014) 838–849, https://doi.org/10.1080/15320383.2014.809049.
[25] J. Cui, W. Li, X. Song, Z. Zhang, H. Yu, W. Shan, Y. Xiong, Microwave-assisted one-pot rapid synthesis of mesoporous silica-chitosan composites for efficient recovery of rhenium(Ⅶ), Sep. Purif. Technol. 277 (2021), 119497, https://doi.org/10.1016/j.seppur.2021.119497.
[26] L. Alcaraz, D. Nathaly Saquinga, F.J. Alguacil, E. Escudero, F.A. Lopez, Application of activated carbon obtained from spent coffee ground wastes to effective terbium recovery from liquid solutions, Metals 11 (2021), https://doi.org/10.3390/met11040630.
[27] I. Ihsanullah, M. Sajid, M. Kabeer, A.M. Shemsi, M.A. Atieh, First investigations on the removal of tungsten species from water using multi-walled carbon nanotubes, Water Air Soil Pollut. 231 (2020) 119, https://doi.org/10.1007/s11270-020-04485-2.
[28] P. Wei, H.J. Lou, X.M. Xu, W.J. Xu, H.Y. Yang, W. Zhang, Y.F. Zhang, Preparation of PP non-woven fabric with good heavy metal adsorption performance via plasma modification and graft polymerization, Appl. Surf. Sci 539 (2021), 148195, https://doi.org/10.1016/j.apsusc.2020.148195.
[29] L. Zhang, J.H. Zhang, X.L. Li, C.J. Wang, A.J. Yu, S.S. Zhang, G.F. Ouyang, Y.Y. Cui, Adsorption behavior and mechanism of Hg (II) on a porous core-shell copper hydroxy sulfate@MOF composite, Appl. Surf. Sci 538 (2021), 148054, https://doi.org/10.1016/j.apsusc.2020.148054.
[30] J. Durisova, L. Jelinek, H. Parschova, E. Mistova, Mutual separation of vanadium and tungsten from aqueous solution via electrochemical reduction and sorption onto chelating resin, Sep. Sci. Technol. 44 (2009) 2750–2760, https://doi.org/10.1080/01496390903135816.
[31] M. Uchikoshi, T. Nagahara, J.-W. Lim, S.-B. Kim, K. Mimura, Anion-exchange behavior of Mo(V) and W(VI) in HCl solutions, High Temp. Mater. Processes 30 (2011) 345–351, https://doi.org/10.1515/htmp.2011.055.
[32] T.H. Nguyen, M.S. Lee, Separation of molybdenum(VI) and tungsten(VI) from sulfuric acid solution by ion exchange with TEVA resin, Sep. Sci. Technol. 50 (2015) 2060–2065, https://doi.org/10.1080/01496395.2015.1007244.
[33] B.A. Masry, J.A. Daoud, Sorption behavior of tungsten and molybdenum on TVEX-TOPO resin from nitric acid solution, J. Chem. Technol. Biotechnol. 96 (2021) 1399–1410, https://doi.org/10.1002/jctb.6660.
[34] A.A. Blokhin, L.G. Kaloshina, N.Y. Lyubman, Y.V. Murashkin, Sorption purification of aqueous ammonium molybdate to remove tungsten impurities with a cation exchanger containing pyrocatechol functional groups, Russ. J. Appl. Chem. 78 (2005) 422–424, https://doi.org/10.1007/s11167-005-0308-x.
[35] M. Gott, B. Ballard, L. Redman, M. Fassbender, E. Birnbaum, K. John, A. Ketring, C. Cutler, S. Jurisson, Radiochemical study of Re/W adsorption behavior on a strongly basic anion exchange resin, Radiochim. Acta 102 (2014) 325–332, https://doi.org/10.1515/ract-2013-2144.
[36] X.-Y. Lu, G.-S. Huo, C.-H. Liao, Separation of macro amounts of tungsten and molybdenum by ion exchange with D309 resin, Trans. Nonferrous Met. Soc. China 24 (2014) 3008–3013, https://doi.org/10.1016/s1003-6326(14)63438-5.
[37] L. Alcaraz, F.J. Alguacil, F.A. Lopez, Microporous adsorbent from winemaking waste for the recovery of Mn(VII) in liquid solutions, Can. J. Chem. Eng. 99 (2021) 447–457, https://doi.org/10.1002/cjce.23862.
[38] M. Li, S. Zhang, S. Cui, K. Qin, Y. Zhang, P. Li, Q. Cao, H. Xiao, Q. Zeng, Pre-grafting effect on improving adsorption efficiency of cellulose based biosorbent for Hg (II) removal from aqueous solution, Sep. Purif. Technol. 277 (2021), 119493, https://doi.org/10.1016/j.seppur.2021.119493.
[39] N.R. Nicomel, L. Otero-Gonzalez, K. Folens, B. Mees, T. Hennebel, G. Du Laing, Selective and enhanced nickel adsorption from sulfate- and calcium-rich solutions

*M.*using chitosan, Sep. Purif. Technol. 276 (2021), 119283, https://doi.org/10.1016/j.seppur.2021.119283.
*MI.*E. Mistova, H. Parschova, L. Jelinek, Z. Matejka, Z. Plichta, M. Benes, Selective sorption of metal oxoanions from dilute solution by chemicaly modified brown seaweed *Ascophyllum nodosum*, Sep. Sci. Technol. 43 (2008) 3168–3182, https://doi.org/10.1080/01496390802215008.
*MII.*E. Mistova, H. Parschova, Z. Matejka, Selective sorption of metal oxoanions from dilute solution by bead cellulose sorbent, Sep. Sci. Technol. 42 (2007) 1231–1243, https://doi.org/10.1080/01496390601174364.
*MIII.*J.Z. Xie, H.L. Chang, J.J. Kilbane, Removal and recovery of metal ions from wastewater using biosorbents and chemically modified biosorbents, Bioresour. Technol. 57 (1996) 127–136, https://doi.org/10.1016/0960-8524(96)00059-4.
*MIV.*Y. Wang, K. Huang, Biosorption of tungstate onto garlic peel loaded with Fe(III), Ce (III), and Ti(IV), Environ. Sci. Pollut. Res. 27 (2020) 33692–33702, https://doi.org/10.1007/s11356-020-09309-8.
*MV.*A.S. Morshedy, A.A. Galhoum, A. Aleem, H. Abdel Aleem, M.T. Shehab El-din, D. M. Okaba, M.S. Mostafa, H.I. Mira, Z. Yang, I.-E.-T. El-Sayed, Functionalized aminophosphonate chitosan-magnetic nanocomposites for Cd(II) removal from aqueous solutions: Performance and mechanisms of sorption, Appl. Surf. Sci 561 (2021), 150069, https://doi.org/10.1016/j.apsusc.2021.150069.
*MVI.*S. Wang, K. Xiao, Y. Mo, B. Yang, T. Vincent, C. Faur, E. Guibal, Selenium(VI) and copper(II) adsorption using polyethyleneimine-based resins: Effect of glutaraldehyde crosslinking and storage condition, J. Hazard. Mater. 386 (2020), 121637, https://doi.org/10.1016/j.jhazmat.2019.121637.
*MVII.*S. Bo, J. Luo, Q. An, Z. Xiao, H. Wang, W. Cai, S. Zhai, Z. Li, Efficiently selective adsorption of Pb(II) with functionalized alginate-based adsorbent in batch/column systems: Mechanism and application simulation, J. Cleaner Prod. 250 (2020), 119585, https://doi.org/10.1016/j.jclepro.2019.119585.
*MVIII.*H.-R. Yang, S.-S. Li, X.-C. Shan, C. Yang, Q.-D. An, S.-R. Zhai, Z.-Y. Xiao, Hollow polyethyleneimine/carboxymethyl cellulose beads with abundant and accessible sorption sites for ultra-efficient chromium (VI) and phosphate removal, Sep. Purif. Technol. 278 (2022), 119607, https://doi.org/10.1016/j.seppur.2021.119607.
*MIX.*Y. Zhang, M.F. Hamza, T. Vincent, J.-C. Roux, C. Faur, E. Guibal, Tuning the sorption properties of amidoxime-functionalized algal/polyethyleneimine beads for La(III) and Dy(III) using EDTA: Impact of metal speciation on selective separation, Chem. Eng. J. (2021), 133214, https://doi.org/10.1016/j.cej.2021.133214.
*MX.*Y. Wei, K.A.M. Salih, K. Rabie, K.Z. Elwakeel, Y.E. Zayed, M.F. Hamza, E. Guibal, Development of phosphoryl-functionalized algal-PEI beads for the sorption of Nd (III) and Mo(VI) from aqueous solutions – Application for rare earth recovery from acid leachates, Chem. Eng. J. 412 (2021), 127399, https://doi.org/10.1016/j.cej.2020.127399.
*MXI.*M.F. Hamza, A.E. Mubark, Y. Wei, T. Vincent, E. Guibal, Quaternization of composite algal/PEI beads for enhanced uranium sorption-application to ore acidic leachate, Gels 6 (2020) 6020012, https://doi.org/10.3390/gels6020012.
*MXII.*M.F. Hamza, K.A.M. Salih, A.A.H. Abdel-Rahman, Y.E. Zayed, Y. Wei, J. Liang, E. Guibal, Sulfonic-functionalized algal/PEI beads for scandium, cerium and holmium sorption from aqueous solutions (synthetic and industrial samples), Chem. Eng. J. 403 (2021), 126399, https://doi.org/10.1016/j.cej.2020.126399.
*MXIII.*S.D. Alexandratos, X.P. Zhu, M. Florent, R. Sellin, Polymer-supported bifunctional amidoximes for the sorption of uranium from seawater, Ind. Eng. Chem. Res. 55 (2016) 4208–4216, https://doi.org/10.1021/acs.iecr.5b03742.
*MXIV.*J. Li, L. Zhu, C. Xiao, L. Chen, Z. Chai, S. Wang, Efficient uptake of perrhenate/pertechnetate from aqueous solutions by the bifunctional anion-exchange resin, Radiochim. Acta 106 (2018) 581–591, https://doi.org/10.1515/ract-2017-2829.
*MXV.*W. Yin, L. Liu, S. Tang, H. Zhang, X. Pan, R. Chi, Facile synthesis of triazole and carboxyl-functionalized cellulose-based adsorbent via click chemistry strategy for efficient Gd(III) removal, Cellulose 26 (2019) 7107–7123, https://doi.org/ 10.1007/s10570-019-02606-7.
*MXVI.*R. Li, X. Tian, I. Ashraf, B. Chen, Fluoride removal using a chelating resin containing phosphonic-sulfonic acid bifunctional group, J. Chromatogr. A 1613 (2020), 460697, https://doi.org/10.1016/j.chroma.2019.460697.
*MXVII.*Y. Wei, M. Rakhatkyzy, K.A.M. Salih, K. Wang, M.F. Hamza, E. Guibal, Controlled bi-functionalization of silica microbeads through grafting of amidoxime/methacrylic acid for Sr(II) enhanced sorption, Chem. Eng. J. 402 (2020), 125220, https://doi.org/10.1016/j.cej.2020.125220.
*MXVIII.*O. Dudarko, N. Kobylinska, B. Mishra, V.G. Kessler, B.P. Tripathi, G. A. Seisenbaeva, Facile strategies for synthesis of functionalized mesoporous silicas for the removal of rare-earth elements and heavy metals from aqueous systems, Microporous Mesoporous Mater. 315 (2021), 110919, https://doi.org/10.1016/j.micromeso.2021.110919.
[58] S.D. Alexandratos, S. Natesan, Ion-selective polymer-supported reagents: the principle of bifunctionality, Eur. Polym. J. 35 (1999) 431–436, https://doi.org/10.1016/s0014-3057(98)00142-6.
[59] S.D. Alexandratos, S.D. Smith, Intraligand cooperation in metal-ion binding by immobilized ligands: The effect of bifunctionality, J. Appl. Polym. Sci. 91 (2004) 463–468, https://doi.org/10.1002/app.13131.
[60] S.D. Alexandratos, X. Zhu, High-affinity ion-complexing polymer-supported reagents: Immobilized phosphate ligands and their affinity for the uranyl ion, React. Funct. Polym. 67 (2007) 375–382, https://doi.org/10.1016/j.reactfunctpolym.2007.01.013.
[61] Y.Q. Wei, J. Qian, L. Huang, D.B. Hua, Bifunctional polymeric microspheres for efficient uranium sorption from aqueous solution: synergistic interaction of positive charge and amidoxime group, RSC Adv. 5 (2015) 64286–64292, https://doi.org/10.1039/c5ra11578g.
[62] M. Piechowicz, C.W. Abney, X. Zhou, N.C. Thacker, Z. Li, W. Lin, Design, synthesis, and characterization of a bifunctional chelator with ultrahigh capacity for uranium uptake from seawater simulant, Ind. Eng. Chem. Res. 55 (2016) 4170–4178, https://doi.org/10.1021/acs.iecr.5b03304.
[63] M.F. Hamza, Y. Wei, E. Guibal, Quaternization of algal/PEI beads (a new sorbent): characterization and application to scandium recovery from aqueous solutions, Chem. Eng. J. 383 (2020), 123210, https://doi.org/10.1016/j.cej.2019.123210.
[64] Y.S. Ho, G. McKay, Pseudo-second order model for sorption processes, Process Biochem. 34 (1999) 451–465, https://doi.org/10.1016/S0032-9592(98)00112-5.
[65] J. Crank, The Mathematics of Diffusion, 2nd. ed., Oxford University Press, Oxford, U.K., 1975.
[66] C. Tien, Adsorption Calculations and Modeling, Butterworth-Heinemann, Newton, MA, 1994.
[67] G. Buema, N. Lupu, H. Chiriac, G. Ciobanu, R.D. Bucur, D. Bucur, L. Favier, M. Harja, Performance assessment of five adsorbents based on fly ash for removal of cadmium ions, J. Mol. Liq. 333 (2021), 1159.
[68] O. Falyouna, O. Eljamal, I. Maamoun, A. Tahara, Y. Sugihara, Magnetic zeolite synthesis for efficient removal of cesium in a lab-scale continuous treatment system, J. Colloid Interface Sci. 571 (2020) 66–79, https://doi.org/10.1016/j.jcis.2020.03.028.
[69] C.F. Baes Jr., R.E. Mesmer, Hydrolysis of Cations, Wiley, NY, 1976.
[70] E. Guibal, Interactions of metal ions with chitosan-based sorbents: a review, Sep. Purif. Technol. 38 (2004) 43–74, https://doi.org/10.1016/j.seppur.2003.10.004.
[71] P.R. Sethuraman, M.A. Leparulo, M.T. Pope, F. Zonnevijlle, C. Brevard, J. Lemerle, Heteropolypentatungstobisphosphonates - cyclopentane-like pseudorotation of an oxometalate structure, JACS 103 (1981) 7665–7666, https://doi.org/10.1021/ja00415a050.
[72] M.A. Hubbe, S. Azizian, S. Douven, Implications of apparent pseudo-second-order adsorption kinetics onto cellulosic materials: A review, BioResources 14 (2019) 7582–7626.
[73] J.-P. Simonin, On the comparison of pseudo-first order and pseudo-second order rate laws in the modeling of adsorption kinetics, Chem. Eng. J. 300 (2016) 254–263, https://doi.org/10.1016/j.cej.2016.04.079.
[74] Y. Marcus, Ion Properties, Marcel Dekker Inc, New York, NY, 1997.
[75] H.N. Tran, E.C. Lima, R.-S. Juang, J.-C. Bollinger, H.-P. Chao, Thermodynamic parameters of liquid–phase adsorption process calculated from different equilibrium constants related to adsorption isotherms: A comparison study, J. Environ Chem. Eng. (2021), 106674, https://doi.org/10.1016/j.jece.2021.106674.
[76] A. Afkhami, T. Madrakian, A. Amini, Mo(VI) and W(VI) removal from water samples by acid-treated high area carbon cloth, Desalination 243 (2009) 258–264, https://doi.org/10.1016/j.desal.2008.04.028.
[77] R.G. Pearson, Acids and bases, Science (New York, N.Y.), 151 (1966) 172-177 (Doi: 10.1126/science.151.3707.172).
[78] H.A. Abu Khoziem, Sequential recovery processes of tungsten from hubnerite mineral concentrate of Qash Amir mineralized quartz veins, South Eastern Desert, Egypt, Physicochem. Probl. Miner. Process. 57 (2021) 91–105, https://doi.org/10.37190/ppmp/141201.
[79] J.F. Paulino, J.C. Afonso, J.L. Mantovano, C.A. Vianna, J.W. Silva Dias da Cunha, Recovery of tungsten by liquid-liquid extraction from a wolframite concentrate after fusion with sodium hydroxide, Hydrometallurgy 127 (2012) 121–124, https://doi.org/10.1016/j.hydromet.2012.07.018.
[80] M.K. Dinker, N.V. Patil, P.S. Kulkarni, A diamino based resin modified silica composite for the selective recovery of tungsten from wastewater, Polym. Int. 65 (2016) 1387–1394, https://doi.org/10.1002/pi.5189.